PRECIPITATION MECHANISMS
IN CONVECTIVE CLOUDS

Thomas William Russell East, M.A., M.Sc.

A Thesis submitted to the Faculty of Graduate
Studies and Research of McGill University
in partial fulfilment of the requirements
for the degree of Doctor of Philosphy

Macdonald Physics Laboratory
McGill University
Montreal

April 12th 1955

TABLE OF CONTENTS

FIGURES

PREFACE

Earlier work.

This thesis surveys precipitation mechanisms; some work by the present writer on two of these mechanisms was submitted earlier as a thesis for the degree of Master of Science at McGill University. Specifically, part of the Introduction, and sections 2.2, 3.1 (in part), 3.2, 3.3 (in part) and 6.2.1 of the present thesis appeared in the M. Sc. Thesis.

At a later stage, a joint paper with Prof. Marshall was accepted for publication by the Quarterly Journal of the Royal Meteorological Society (East and Marshall, 1954). Parts of the present thesis which appeared in the paper, but not in the M. Sc. Thesis, are sections 2.3, 3.4 (in part), and part of the Introduction.

All the sections not mentioned appear herein for the first time, and in particular, sections 4, 5, 7, 8, and 9, and the three Appendices, and most of the numerical results of sections 3 and 6 are entirely new.

Acknowledgements

The writer is greatly indebted to Professor J. S. Marshall for suggesting the subject of this thesis, and for his encouragement and helpful advice in the course of the work.

The Stormy Weather Research Group, under Dr. Marshall's direction, provided a stimulating and congenial atmosphere, and many helpful discussions were held. In particular, the writer is grateful to Walter Hitschfeld for advice on fall and collision of water drops, to R. H. Douglas for interpretation of upper air data and similar assistance, and to Roger l'Hermitte, visiting from Meteorologie Nationale (France) for reading through section 4, and to G. K. Batchelor for criticising section 7.

Thanks are due to Eva Reiner for performing many of the numerical calculations with speed and accuracy, to Mrs.Constance Slinn for preparing the ink drawings from which the figures were made, and to Mrs. Berta Nemenoff for typing the manuscript.

The work reported in this thesis was made possible through the support and sponsorship of the Geophysical Research Directorate of the U. S. Air Force Cambridge Research Center under Contract No. AF 19 (122)-217.

1. INTRODUCTION

The past decade has seen an increasing interest in the problem of rainfall from convective clouds. It has been stimulated by the recognition that the mechanism must differ fundamentally from that in layer clouds.

Bergeron's (1933) theory, with modifications by Findeisen, is the generally accepted mechanism of precipitation from stratiform clouds. He showed that ice particles can grow rapidly in supersaturated water cloud, then melt and fall as rain. This explanation, which has received ample experimental confirmation, tended to get carried over to precipitation from convective clouds. The fact that in temperate latitudes a towering cumulus often reaches a sufficient height to glaciate has led to the assumption that glaciation is the main precipitation mechanism in cumulus as it is in layer clouds (Byers and Braham, 1949).

Glaciation can play a significant part, as shown by the occurrence of hailstorms, but it is not always present, and the range of heights at which glaciation can be expected does not seem to coincide with the region where precipitation is first observed by radar. The onset of precipitation in a cumulus cloud originates at a point considerably below the top, and spreads rapidly in vertical extent. (Battan (1953) found the temperature at the centre of the first echo averaged $+5^{o}C$ in Ohio thundershowers, and even at the top of the first echo it averaged $+0.5^{o}C$). Indeed, particularly in tropical regions, rain often falls from clouds which lie entirely below the $0^{o}C$ level, as reported by Hunt (1949), Virgo (1950) and E.J. Smith (1951). Mordy and Eber (1954) made an extensive investigation of showery cumulus near Hawaii, finding that raindrops of up to 2 mm diameter fell from clouds whose tops were no colder than $+7^{o}C$.

If droplets of radius 40 microns, or of that order, develop in a cloud (and they are often found in large numbers in Cumulus Congestus and Cumulonimbus), their calculated rapidity of growth is sufficient to produce precipitation. To explain the rapid spread in vertical extent that is observed, it is probably necessary to assume the appearance of drops of such size almost simultaneously over a considerable range of heights.

Ludlam (1951) and others have shown that these initial large droplets could be caused by condensation on to giant salt nuclei. While this approach can reasonably account for the number of raindrops (a few thousand per cubic metre) observed, it cannot account for the several million growing cloud droplets per cubic metre in precipitating Cumulus. Any mechanism which produces the observed cloud droplet size distribution is a potential precipitation mechanism, but the converse is not always true.

In this thesis, various processes will be examined for their ability to grow a considerable population of large droplets in a cloud which, when freshly formed, is almost completely free from them. It was shown in the M.Sc. Thesis (East 1953) and it will be shown in further detail in section 3 that the required growth cannot be produced by gravity alone. The assistance to be expected from electric charges on the droplets is discussed in section 4.

Howell (1949) discussed the growth of droplets by condensation, but he was concerned with the initial formation of clouds rather than their later development. His methods are used in section 5 below to show that the condensation process alone would not lead to precipitation, but that in certain circumstances a combination of condensation and gravity would favour rapid growth.

The possibility of turbulence playing some part in the precipitation process has been considered by other writers. Be rgeron (1933) concluded it would not be intense enough to do so in stratiform clouds, but did not discuss its action in cumuliform clouds. Arenberg (1939) considered the action of turbulence in causing water droplets to be thrown together, without taking account of the conditions necessary for them actually to collide. Mason (1952) introduced turbulence to prolong the paths travelled by droplets through a cloud in becoming drizzle, and Best (1952) to transport them to and from the centre of a cloud. Gabilly (1949) considered its effect in causing collisions, but confined his discussion to sinusoidal motion of the air, rather than true turbulence, which is a random motion.

In the M.Sc. Thesis, Gabilly's approach was carried further to include the random character of turbulent motion. In section 6 below these methods are applied to show the effect on a cloud. In section 7 the available experimental data on turbulence in clouds is examined quantitatively; it seems to show that it does not normally have sufficient intensity to initiate the precipitation process.

In undertaking to assess the relative importance of these possible precipitation mechanisms, lack of certain knowledge on detailed points was never allowed to hold up the work. Physically reasonable assumptions were made where necessary, and these can be justified in many cases.

The most probable mechanism, on present showing, appears to be one in which a parcel of cloud ascends on the wet adiabatic, and then rests at constant level. Gravity is then an efficient precipitation mechanism. This concept fits well with the latest views of cloud convection.

2. CONVECTIVE CLOUDS

2.1 Macrostructure.

A cumulus cloud is convective in nature. Some parts of it are in upward motion; in these regions the rising air expands and cools, forcing the water vapour present in it to condense into liquid water. The latent heat released by condensation is the source of energy for maintaining the upward motion against drag.

On the accepted model, a cumulus cloud consists of one or more "cells", each having a central updraft with an average vertical velocity of a few metres per second (Byers and Braham, 1949). The rising column of air mixes with the environment by a process of "entrainment". Malkus (1954) found that an aircraft can cross and recross an updraft, following it up through all levels of the cloud.

Scorer and Ludlam (1953), on the other hand, suggested that the updrafts in a cloud are discontinuous, each consisting of a series of "bubbles" of air warmer than the surrounding cloud mass. Their hypothesis was supported by the experience of glider pilots, and, at least in the upper part of a cloud, by motion picture studies. Malkus and Scorer (1955) have developed a satisfactory theory giving good agreement with the observations.

Batchelor (1954), in a series of analogue experiments, showed that a mass of fluid retains its identity only if it differs considerably in density from the surrounding fluid.

On this basis one would not expect Ludlam and Scorer's "bubble" to survive for an appreciable time in the cloud. Batchelor's experiments, however, did not take into account the local source of energy represented by the latent heat of condensation of water; it might conceivably ensure a longer life for the "bubble".

Whether the updraft is really steady or consists of a series of bubbles, the following influences must be at work on the cloud-filled air: condensation of water vapour, mixing of air parcels with different histories and properties, shear which produces turbulent motion, and the earth's gravitational field. The effects of some of these influences will be studied in isolation and in combination, and the results considered in relation to the cloud structure.

2.2 Microstructure

A discussion of precipitation mechanisms must start from the number and sizes of water droplets in the cloud. Measurements of these quantities have been made from aircraft and the results described by Diem (1942, 1948), Zaitsev (1950), and Weickmann and aufm Kampe (1953). Droplet-size distributions, that is the fraction of the liquid water contributed to the total by droplets of various sizes were measured directly by catching the droplets in a film of oil and photomicrographing them. The total liquid water content per unit volume, W, was measured directly by Diem and Zaitsev, and determined indirectly from measurements of optical transmission by Weickmann and aufm Kampe. The total number of droplets per unit volume, N, can then be computed.

A noticeable feature of the published distributions is the almost complete absence of droplets of less than 3 microns radius. The oil-slide method is incapable of detecting droplets of less than 2 microns radius or so. If there were a population of small droplets which escaped detection comparable in number with those detected, serious errors might result when converting from transmission to water content, and of course the values of N would be quite wrong in any case. This point was discussed at length by Fritz (1954). aufm Kampe and Weickmann (1954), however, point out that the condensation process by which the droplets are formed in the first place inhibits the production of very small droplets once a population of moderate-sized droplets has developed. Howell's (1949) computations and section 5 of this thesis bear out the conclusion that there really are practically no droplets of 3 microns radius or less.

Weickmann and aufm Kampe measured only convective clouds; the data* include the distribution of the number of droplets with radius, together with the total number of droplets per cm^3, N, and the liquid water content, W. In figure 2.1 N is plotted against W for the 34 samples. If we combine the Cumulus Humilis and Cumulus samples and call them Fair-weather cumulus, we see that they are clearly separated in the figure from the Cumulonimbus and Cumulus congestus samples, which we can call Heavy cumulus. Fair-weather cumulus have large numbers of droplets but small water content, while heavy cumulus have roughly one-

*Private communication from aufm Kampe and Weickmann, Evans Signal Corps Laboratory, New Jersey.

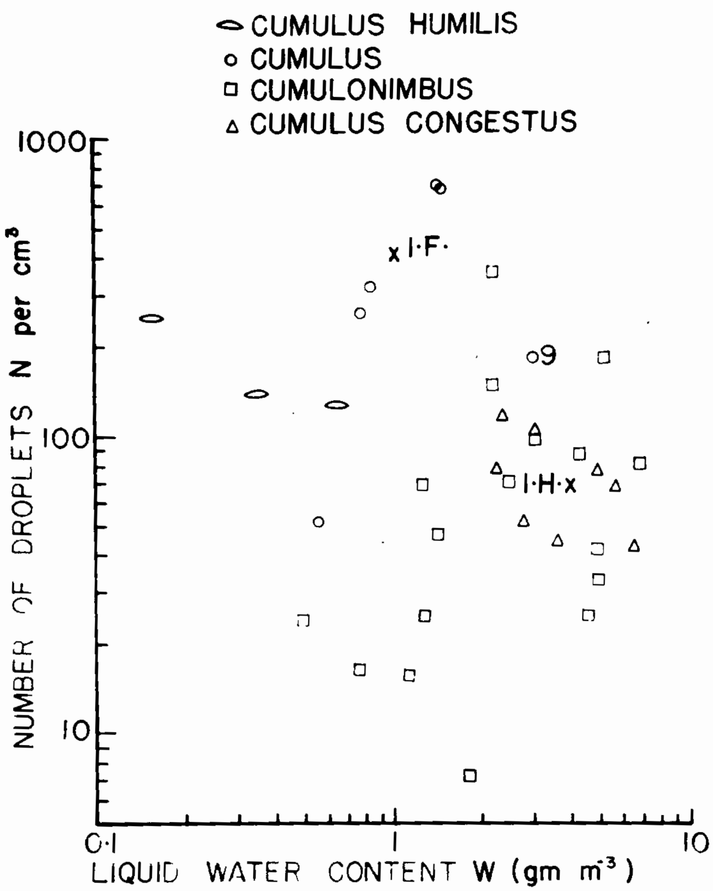

Figure 2.1 Properties of cumulus clouds (measured by aufm Kampe and Weickmann). Total number of droplets per cm^3 versus water content for each specimen.
I.F. Idealised fair-weather cumulus.
I.H. Idealised heavy cumulus.

sixth the number of droplets but about four times the water content. Sample number 9, however, appears to be an exception.

A survey of the distribution curves showed that (excepting no.9) fair-weather clouds are free from droplets of more than about 20 microns radius and in many cases have none greater than 18 microns radius.

The drop size distributions of a number of cumulus clouds were replotted on logarithmico-normal charts (as described by Kottler (1950, 1951, 1952)). Some of the plots for fair-weather cumulus are reproduced in figure 2.2(a). The steepness of the curves indicated the narrowness of the distributions and their straightness showed that they were good approximations to log-normal distributions. One of aufm Kampe and Weickmann's (figure 2.2(a), no.9) is an exception. The plots for heavy cumulus (some of which are reproduced in figure 2.2(b) show much broader, and in some cases, bimodal distributions, that is, distributions made up of two log-normal distributions with different madian radii. Bimodality appears also to be a property of specimen no. 9: in view of the other anomalous properties of this specimen already noted, this justifies its exclusion from the fair-weather category.

A few words may usefully be said about average distributions at this point. If aufm Kampe and Weickmann's fair-weather distributions, excluding no. 9, are combined to make an <u>average</u> curve, the result is also a <u>typical</u> curve, cutting off at about 20 microns radius. An average curve which in-

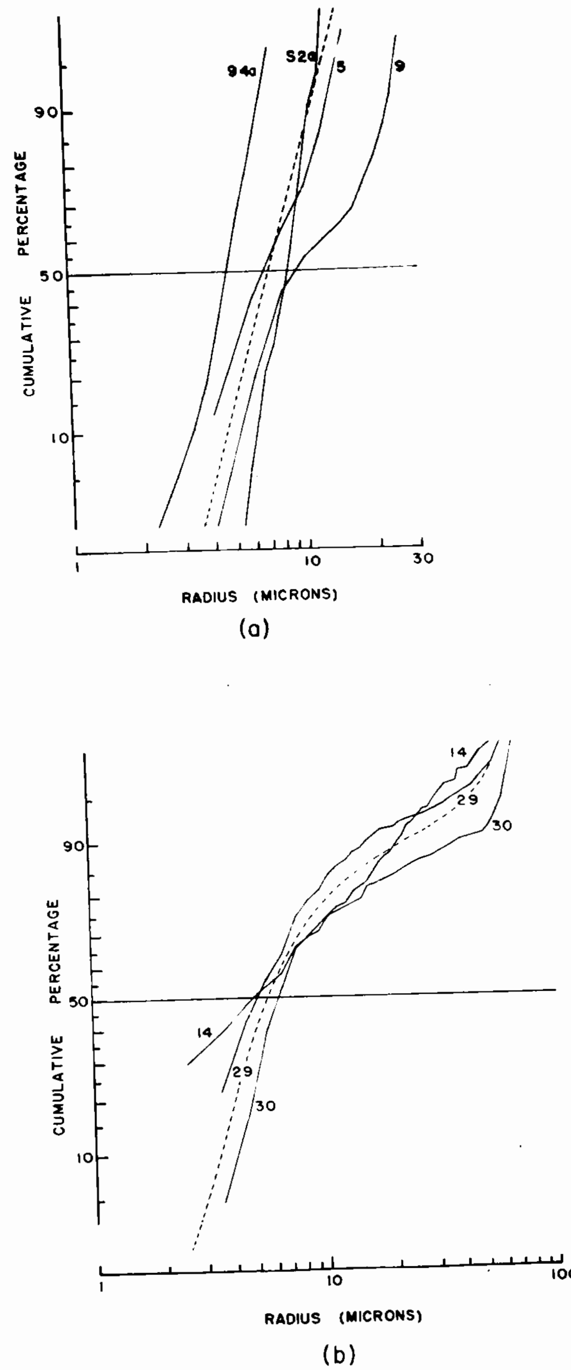

Figure 2.2 Droplet size distributions on cumulative percentage log-normal charts. The ordinate is the percentage number of droplets of radius less than the abscissa.
(a) Fair weather cumulus: 94a, 52a, Diem; 5, 9, aufm Kampe and Weickmann.
(b) Heavy cumulus (aufm Kampe and Weickmann): 14, 29, cumulo-nimbus; 30, cumulus congestus.
The dashed curves are idealised distributions.

cludes no. 9, however, is not typical. The unusually large droplets introduced by this specimen do not affect the total number appreciably, but any quantity which increases very rapidly with radius, such as radar reflectivity (which goes as r^6), or rate of growth by coalescence (see section 3) will be misleadingly exaggerated in the average result.

In the M.Sc. thesis an idealised fair-weather distribution was described, which is shown as a dashed line on figure 2.2.(a). The starting-point of the present work is the distribution

$$\left.\begin{aligned} n(r)\,dr &= \frac{486}{r}\exp\left\{-22\left(\log_{10}\frac{r}{7}\right)^2\right\} & r \leq 18 \\ n(r) &= 0 & r > 18 \end{aligned}\right\} \quad (2.1)$$

where $n(r)dr$ is the number of droplets per cm^3 whose radii lie between r and $r + dr$ microns. It differs from the distribution used in the M.Sc. thesis in having a sharp cut-off at 18 microns radius and in the water content W being then normalised to 1 g m^{-3}. The total number of droplets per cm^3, N, is 420; these values are plotted on figure 2.1 as the cross "I.F."

The idealised fair-weather distribution is replotted as as a water-content distribution in figure 2.3 (left-hand curve). Here $w(r)dr$ is the amount of liquid water in unit volume of cloud-filled air which consists of droplets whose radii lie between r and $r + dr$ microns. It is assumed that in the early stages of development (or at a position in the cloud near its base) a convective cloud which eventually precipitates had the

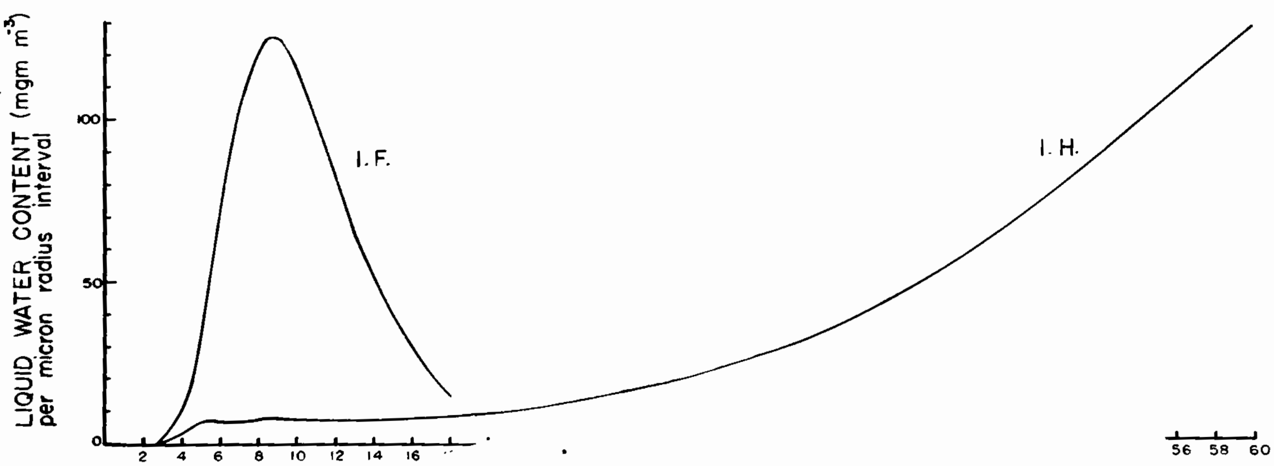

Figur .3 Iealis roplet size distributions. Liquid
water ntn versu raius, corresponding to the dashed
lines figre 2.
I.F. palis fa-wether cumulus.
I.H. palisd hey cmulus.

same microstructure as a fair-weather cumulus. The idealised distribution was therefore used as the starting point for all calculations described in this thesis.

For eventual comparison with the results of the calculations an idealised heavy cumulus distribution has been derived by drawing the dashed curve on figure 2.2(b), assigning to it a water content $W = 4$ g m^{-3} and converting it to a water content distribution. It appears as the steadily rising curve on figure 2.3; this curve shows very clearly that most of the water content of heavy cumulus clouds is in the form of large drops. The curve should be regarded as only approximate, since between 50 and 60 microns it becomes extremely sensitive to minor details of behaviour of the upper end of the cumulative curve of figure 2.2(b). The total number of droplets comes out to $N = 70$ cm^{-3}; the position on the chart of figure 2.1 is marked by the cross "I.H."

2.3 Condensation and Coalescence.

It is clear from figure 2.1 that between the earlier and the later stages of the cloud's history, several grams of liquid water per m^3 have been added to the cloud. This must have been condensed from the vapour, and the effect on the droplet size distribution will have to be considered in section 5.

Howell's (1949) results show that by the time the liquid water content reaches 1 g m^{-3}, condensation from the vapour cannot increase the number of droplets appreciably. On the other hand it certainly cannot decrease the number of droplets. In the absence of the ice phase, coalescence of droplets is the only way the number can be reduced (apart from evaporation). The marked decrease in numbers shown in figure 2.1 in going towards the heavy cumulus samples is important evidence that some coalescence process is taking place.

3. COALESCENCE BY DIFFERENTIAL SETTLING

3.1 Velocities of fall

Cloud droplets fall relative to the air in which they find themselves, with terminal velocities which depend on their size. As the larger droplets fall, they approach any smaller ones which lie in their path. Some collisions occur, and the larger droplets grow at the expense of the smaller ones. This basic coalescence mechanism takes place in almost any cloud all the time, so it will be investigated before any other possible process. Since the probability of occurrence of collisions depends rather critically on relative velocity, we have first to discuss terminal velocities.

In the troposphere, the terminal velocity of water droplets of radius r less than 18 microns is given within 1 percent by a formula derived from Stokes' Law, namely

$$v_r = g_E \frac{2\rho_s r^2}{9\eta} = g_E \tau_r \qquad (3.1)$$

where g_E = earth's gravitational field = 980 cm sec^{-2}

$\tau_r = 2\rho_s r^2/9\eta$, the "time constant" of the droplet

and η = dynamic viscosity = 1.72×10^{-4} g cm^{-1}sec^{-1}at 0C.

$$\text{or } v_r = 1.266 \times 10^{-2} r^2 \qquad (v_r \text{ in cm sec}^{-1}, \text{ r in microns}) \qquad (3.1)$$

(The temperature and pressure vary throughout the cloud, but in this thesis air is taken to have the constant properties $\rho = 0.96 \times 10^{-3}$g cm^{-3} and $\eta = 1.72 \times 10^{-4}$g cm^{-1} sec^{-1}. These are the values for 0°C and 760 mb, roughly the conditions in which precipitation first forms in temperate latitudes.)

Cunningham (1910) showed by the Kinetic theory of gases that the average terminal velocity of very small droplets must be greater than this by the factor $(1 + 1.63\ell/r)$ where ℓ = mean free path = 0.12 microns at 760 mb and 0C. The factor amounts to 1.049 for the terminal velocity of a 4 micron droplet. However, we shall need the relative velocity $U = v_s - v_r$ between a drop s and a droplet r. It can be shown that the percentage correction in U goes as $(s + r)^{-1}$. The largest percentage correction required in the present work would be for $s = 13\frac{1}{2}$, $r = 4$ microns where it is 1.1 percent. The correction was therefore neglected entirely.

The molecular nature of air gives rise to Brownian motion of small particles in it. The mean energy of translation of the particle is $\frac{3}{2}$ kT, so that for a water droplet of radius 4 microns at 0C the root mean square velocity is 0.205 cm sec^{-1}; it is proportional to $r^{-3/2}$. The relative velocities with which we will be concerned are at least 12 times as great for this size of droplet. It will appear in section 6.2 below that even a random velocity as great as the steady relative velocity has only a moderate effect on coalescence, so the effect of Brownian motion has been neglected.

The molecular character of air was neglected in two other instances. Langmuir's theory of droplet collisions used in section 3 and the turbulence theory applied in section 7 both assume that the air has its bulk properties on the scale of their respective processes. The appropriate scale in the collision process is the radius of the droplet (4 microns or more), and in turbulent motion it is the size of the smallest eddy (which is of the order 1 mm. in a cumulus cloud, according to the estimates of section 7 below). The mean free path, ℓ, is very much less than either of these quantities, so there seems no reason to suspect any appreciable effect on the two processes.

At radii above 18 microns the Reynolds number R at the terminal velocity becomes appreciable and Stokes' Law is not accurate. The value of terminal velocity given by equation (3.1) is too large and must be multiplied by a factor φ. The experimental relationship between drag coefficient and Reynolds number given by Schiller (1932) was used to compute φ for the terminal velocity of a drop of any radius s by a method of successive approximations. (See Appendix 3(b) for further discussion. The factor φ is plotted in figure A3.1; the abscissa is drag force, but the subsidiary scale immediately underneath shows the radius for which φ is appropriate for calculating terminal velocity). For example, a drop, radius $s = 100$ microns, has a terminal velocity 0.6 times the value given by equation (3.1).

3.2 Langmuir's equation

A drop, radius s, terminal velocity v_s, sweeps out a volume $\pi s^2 v_s$ in unit time. If it fell through a monodisperse, randomly distributed population of droplets, radii r, terminal velocity v_r, and if all the droplets continued in a straight line in unit time, the drop would collide with all the droplets in a volume $\pi(s+r)^2 U$, where the relative velocity $U = v_s - v_r$. We define the "encounter cross-section" as $\pi(s+r)^2$.

Since the droplets do not continue in straight lines, but tend to be brushed aside by the drop, the actual number of collisions is less. In the M.Sc. Thesis, the encounter cross section was replaced by a "collision cross-section" $E\pi(s+r)^2$, where E is the "collision efficiency" defined and computed by Langmuir (1948). In applying Langmuir's work to the problem the following assumptions were made:

1. Langmuir's theory, worked out for droplets much smaller than the drop, is still applicable when the radii are more nearly equal.
2. It applies despite appreciable motion of the droplets through the air, if use is made of the relative velocity U.
3. The theory also applies when the velocities are not steady.
4. Collisions always lead to coalescence. Justification for this is discussed in the M.Sc. thesis.

These assumptions are carried over into the present work.

The efficiency E (corresponding to Langmuir's E_v) is always less than unity, and can be zero. It is a unique, monotonic function of a dimensionless parameter $K = U\tau_r/s$, where $\tau_r = 2\rho_s r^2/9\eta$; the equation is

$$E = 0, \qquad K < 1.214,$$

$$E = \left[1 + \frac{\frac{3}{4}\ln(2K)}{K - 1.214}\right]^{-2}, \qquad K > 1.214$$

(3.2)

(This relationship is reproduced in figure 6.2, in section 6 below).

Sartor (1954) has performed an interesting series of experiments on large water drops in oil. Regarded as scale model experiments on cloud droplets, they appear to show that collisions can occur more readily, but coalescence less readily, than Langmuir's equation would indicate: electric fields occurring in nature would greatly increase the probability of coalescence.

The observed stability of fair weather cumulus tends to confirm the prediction of Langmuir's equation that coalescence between droplets in such clouds is rare. The choice between accepting either the results of Sartor's scale model, analogue experiment, or an extrapolation of Langmuir's experimentally verified (Gunn and Hitschfeld 1951) theory, was made in favour of the latter; Langmuir's equation is used throughout the following work.

3.3 Growth of drop

Consider a population consisting of those cloud droplets having radii between r and r + dr. Its water content is w(r)dr. The rate at which water is swept up by a drop, radius s, falling through it (which is the rate of increase of mass m_s of the drop due to this particular population) is

$$\left[\frac{dm_s}{dt}\right]_r dr = \pi (s+r)^2 . VE . w(r) dr$$
$$= Q(s,r) . w(r) dr \qquad (3.3)$$

We define the "equivalent volume sweeping rate" Q(s,r) $= \pi(s + r)^2$.UE; it has the dimensions of volume per unit time and is shown in figure 3.1.

It was pointed out in the M. Sc. Thesis that when s = 15 microns, collisions are not possible with droplets less than 15 microns , except for radii between 9 and 13 microns, where they are still relatively rare. Figure 3.1 shows that by the time s = 30 microns, collisions are possible with most droplets, and in the case of 10 micron droplets they are over 100 times more frequent than they were at s = 15 microns. The main reason for this remarkable increase is that the relative velocities between the 15 micron drop and the droplets were so small that, for most droplets, K was less than 1.214 so that E was zero.

The rate of increase of mass of the drop as it sweeps up the cloud is

$$\frac{dm_s}{dt} = \int_0^s \left[\frac{dm_s}{dt}\right]_r dr = \int_0^s Q(s,r) . w(r) dr \qquad (3.4)$$

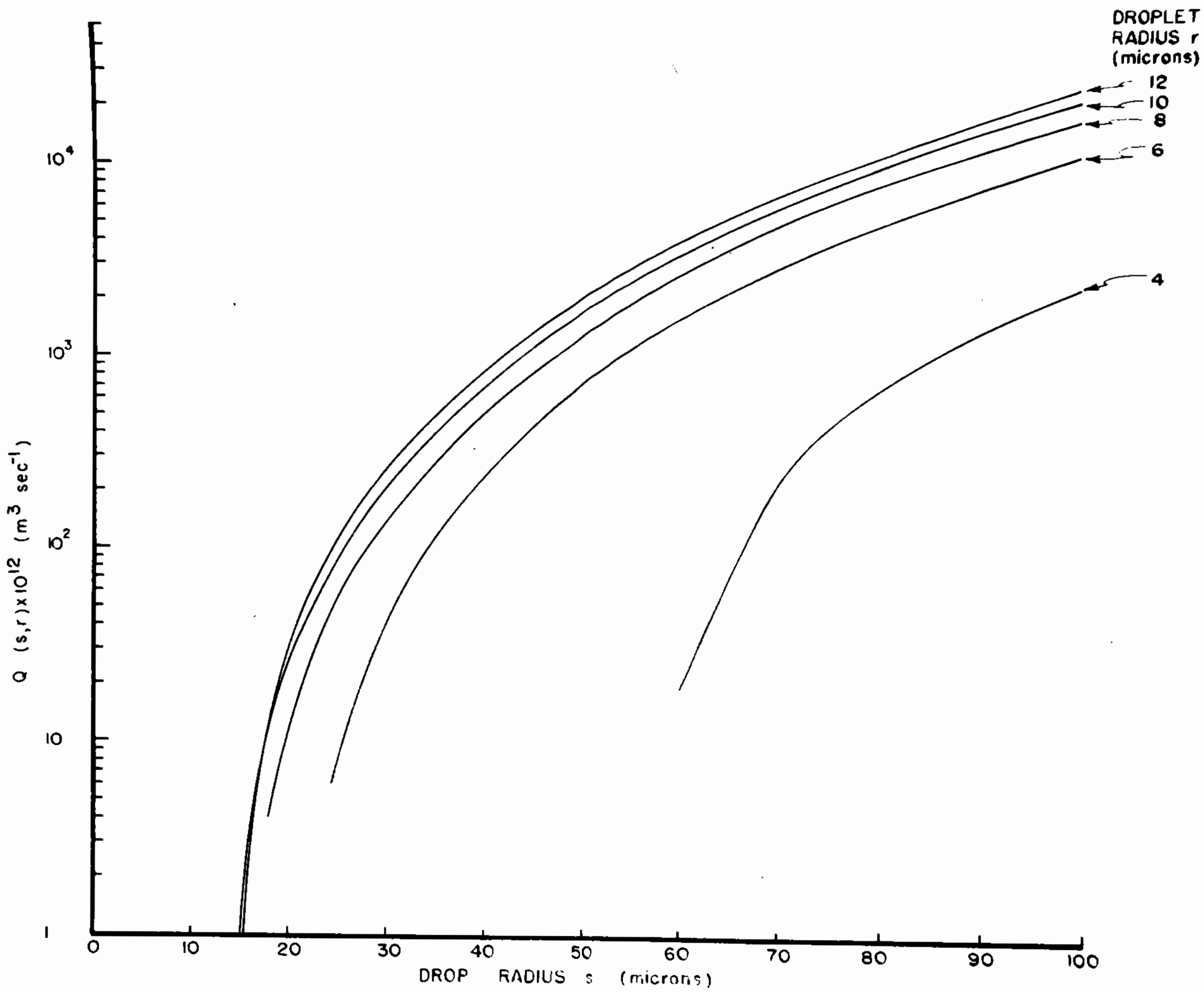

Figure 3.1 Equivalent volume sweeping rate (gravity alone). The quantity Q(s,r) versus drop radius s, for the droplet radius r shown on curve.

The numerical method used to evaluate this integral is described in Appendix I.

The way in which the total dm_s/dt is made up from droplets of various radii is shown in figure 3.2. Here $[dm_s/dt]_r$ is plotted against r at various stages in the growth of the drop; the curves are normalised to an area of 100 percent by dividing each by its own dm_s/dt. The shape of any curve is determined partly by the relative values of $Q(s,r)$ for various values of r (compare particularly the small values at $r = 4$ with the depressed curve for $r = 4$ in figure 3.1), and partly by the cloud droplet size distribution $w(r)$; the idealised fair-weather distribution (I.F.) was used. It was assumed in the calculation that $w(r)$ was independent of time, and therefore of s, (i.e. that negligible depletion took place). In the result, the curves are all much alike, except for small s. In particular, at $r = 9$ microns, the ratio of $[dm_s/dt]_r$ to dm_s/dt is almost independent of s; use was made of this fact to speed up the calculation of dm_s/dt over part of the range of s.

The computed values of dm_s/dt as a function of s were converted to s as a function of t by a numerical method described in Appendix 1. Figure 3.3 shows how the drop radius s increases with time as it falls through the cloud. Zero of time is taken at $s = 17$ microns, and growth

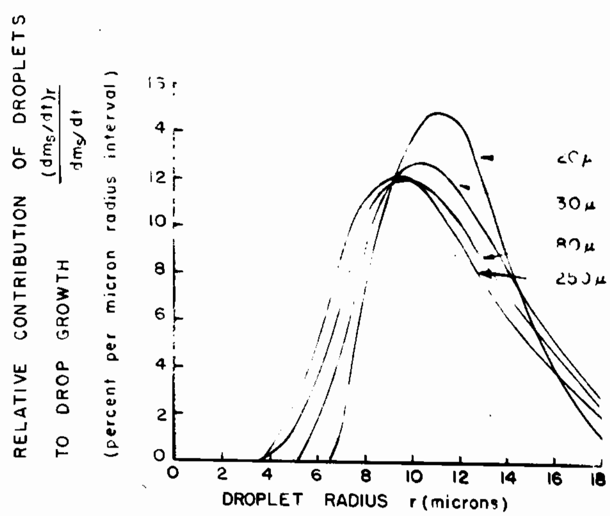

Figure 3.2 Relative contributions of droplets to growth of drop. Percentage of dm_s/dt contributed by droplets of radius r (per micron) versus r, as drop of radius s falls by gravity through I.F. cloud.

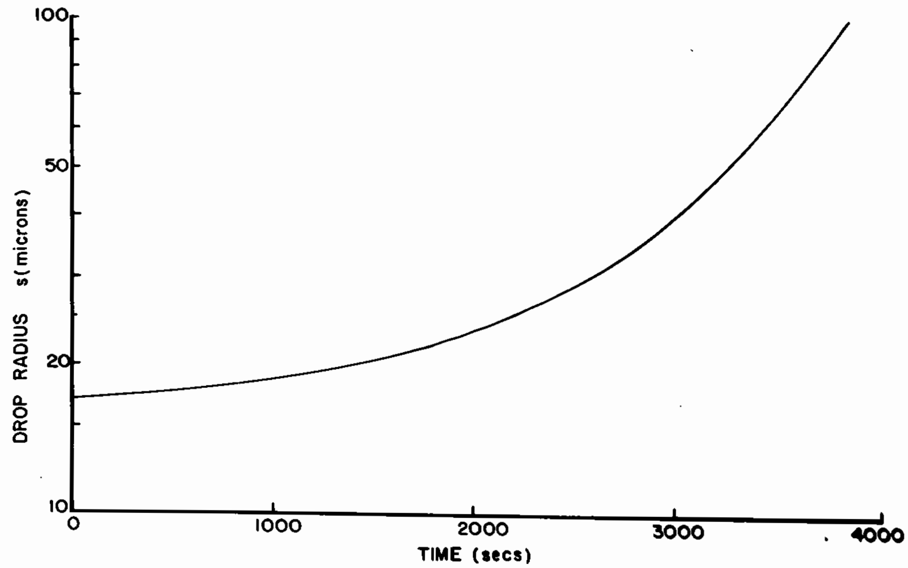

Figure 3.3 Growth of drop by coalescence (gravity alone).
Drop radius versus time, as the drop falls through I.F. cloud.

is followed out to $s = 100$ microns, i.e. drizzle drop size; the whole process takes over an hour, half of which is spent in going from 17 to 23 microns radius.

The growth curve of figure 3.3 applies in the idealised fair-weather cloud whose water content is 1 g m^{-3}. Rate of growth is directly proportional to number of collisions, so that for a drop falling through a cloud of liquid water content W g m^{-3} but the same droplet size distribution as the I.F. distribution (and therefore W times as many droplets), all times would be decreased by the factor W.

3.4 Modification of droplet-size distribution

The problem of precipitation mechanisms is a problem of droplet growth mechanisms. An important piece of evidence is the change in droplet-size distribution between the early and mature stages of a cloud (figures 2.2 and 2.3). Any suggested growth mechanism can be tested by computing its effect on the droplet-size distribution, then comparing the theoretical and experimental curves; the change must be brought about in a realistically short time, say half an hour, sometimes more, often less.

The analysis of the previous sub-section is adequate to follow the growth of a few outstandingly large drops, in a cloud of many droplets. In producing a heavy cumulus distribution from a fair-weather, however, the major part of the water content has gone over from the smaller droplets to the larger. Depletion of the droplet population and competition for the available water among the growing droplets cannot be neglected.

An added complication is the possibility that a particular droplet may grow for a while by sweeping up smaller droplets, and then itself be swept up by a larger droplet. To keep the labour of the computation within bounds, it was decided to ignore this possibility when computing the modification of droplet-size distributions by coalescence, and to set up the following convention:

> Particles greater than 13 microns radius are called <u>drops;</u>
>
> Particles less than 13 microns radius are called <u>droplets:</u>
>
> Collisions can only take place between a drop and a droplet.
>
> At each collision the number of droplets decreases by one, and the mass of the drop increases by the mass of the droplet.

In the computations the radius of a droplet is called $r(<13)$ and the radius of a drop is called $s(>13)$.

The method of computation is to start with the I.F. distribution and divide it up into drops and droplets. Now calculate the growth of all the drops as they sweep up the droplets for a limited time Δt; then find by how much the droplets have been depleted in that time. The computation proceeds step by step in this way until the largest drops have grown from 18 to about 40 microns radius (5 steps in all). Details of the method are given in Appendix 1(b).

In figures 3.4 and 3.5, the radii r and s are plotted continuously along the horizontal axis. The discontinuity at 13 microns is due to the convention above. Droplet-droplet collisions are impossible anyway with gravity alone (M.Sc. Thesis), but drop-drop collisions would have reduced the peak between 13 and 15 microns and slightly increased the rates of growth of the larger drops.

Evidently it would take nearly two hours for a fair-weather cumulus to mature if gravity were the only agency. Such a time scale seems more appropriate to the ageing of stratus or fog; a vigorous cumulus cloud develops much faster than this.

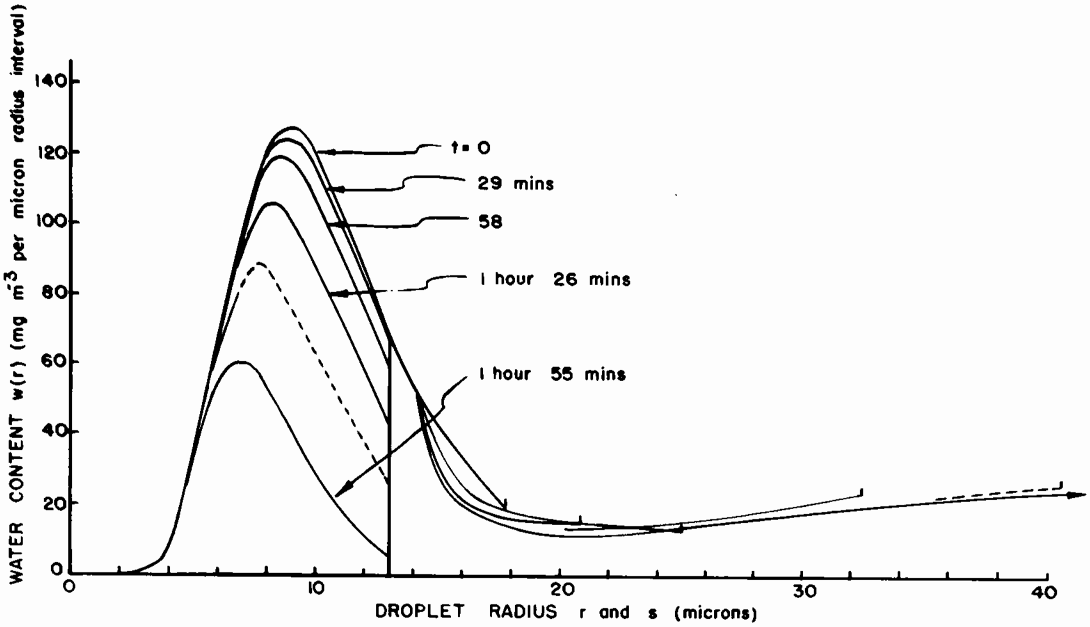

Figure 3.4 Modification of water content distribution by coalescence (gravity alone). The curve $t = 0$ is for I.F. cloud. Drops larger than 13 microns are allowed to sweep up droplets smaller than 13 microns: the curves for later times show the result. (Between 14 and 20 microns several of the curves almost coincide. In this region only the curves for $t = 0, 29$ and 58 mins. and 1 hr 55 mins. are shown). After 1 hr 55 mins. (lat curve) the largest drops reach 49 microns.

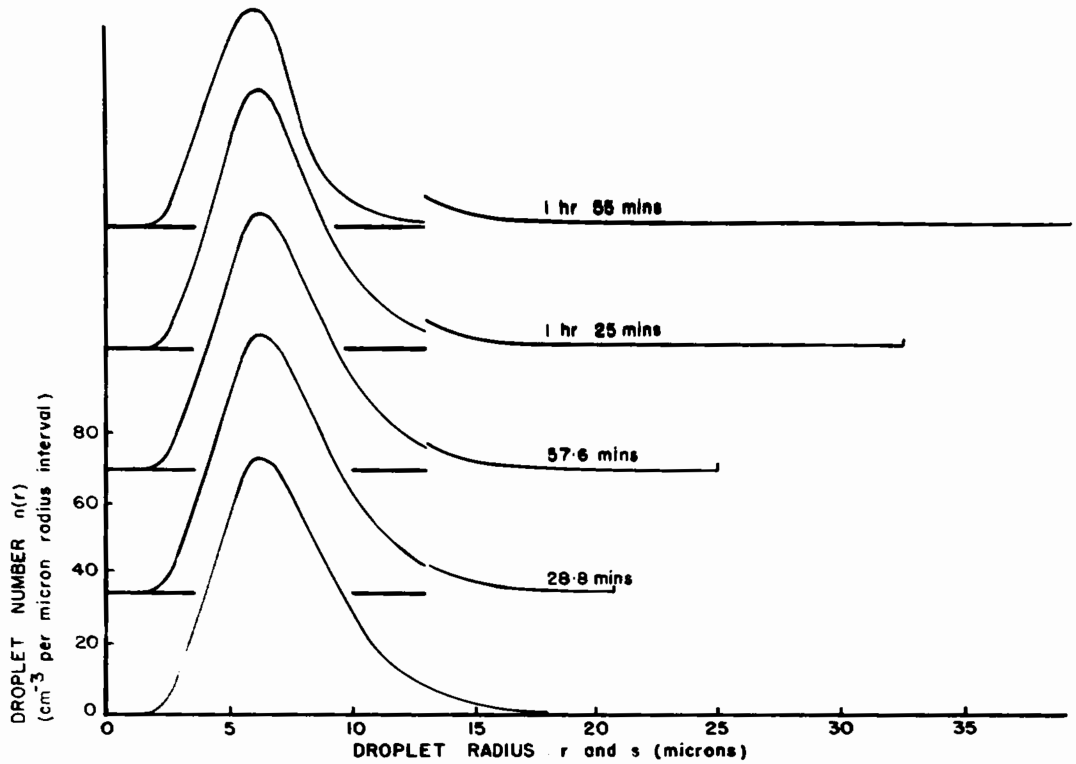

Figure 3.5 Modification of droplet number distribution by coalescence (gravity alone). The lowest curve is for I.F. cloud. The vertical displacement is for clarity only. The break in the curves at 13 microns is due to the artificial restriction on collisions.

4. THE EFFECT OF ELECTRIC CHARGE ON COALESCENCE

4.1 Magnitude of charge

The force of attraction between oppositely charged droplets would assist coalescence in a cloud, and has to be considered as a possible factor in bringing about precipitation in cumulus. A charged droplet will also attract neutral ones, though the force is much weaker.

Cochet (1952) considered a cloud of neutral droplets of radius 8μ, with water content 2 g m^{-3}; he showed that a droplet of radius 15μ carrying a charge of 4.10^{-4} e.s.u. would grow very rapidly by coalescence. This charge, however, is equivalent to about 800,000 electrons; it might arise in artificial seeding but seems much too large to be found in a warm cumulus in the early stages of precipitation.

Ross Gunn (1954) calculates that an isolated drop of 15μ radius would collect, on the average, about 100 electronic charges in neutral air. The proximity of other droplets, however, decreases the charge collected by each one. In a private communication, Dr. Gunn reports that the mean equilibrium charge on each droplet would approximate 19 elementary units, at a radius of 15 microns.

4.2 Force of attraction

Calculation of the exact force between two droplets carrying equal and opposite charges becomes very difficult when the distance between them is not large compared with their radii. One possible approach, which requires rather bold assumptions, uses the concept of image charges described by Stratton (1941).

Figure 4.1 shows how the charge $-q$ on a droplet appears to be drawn to a point near the surface by a point charge $+q$ just outside. This picture is transferred to the case of two oppositely charged droplets in figure 4.2 where the charges have attracted each other into symmetrical positions. The distance between the charges $D \doteqdot (4r_1\, d)^{1/2}$ when the distance between the droplet surfaces is d if the approach is close. The attractive force

$$f = \frac{q^2}{4\pi D^2} = \frac{q^2}{4\pi . 4 r_1 d} \tag{4.1}$$

Putting $q = 19 \times 4.8 \times 10^{-10}$ e.s.u., $r_1 = 15 \times 10^{-4}$ cm., and supposing for example that the droplets are only 0.2 microns apart, so that $d = 2 \times 10^{-5}$ cm, we find $f = 55 \times 10^{-12}$ dyne.

4.3 Effect on collisions

Suppose the two droplets have radii which are about 15 microns but which differ sufficiently for their relative velocity when falling freely to be $U = 0.625$ cm sec^{-1}. This is the value for which Langmuir's parameter $K = 1.214$, so that (setting aside once more the question of validity for nearly equal particles) at best only grazing incidence can occur under the action of gravity alone. The force F would produce a radial

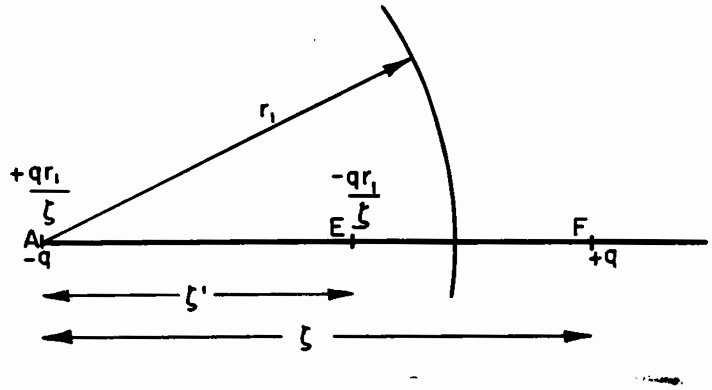

Figure 4.1 Method of images. The conducting sphere, centre A, radius r_1, carries a charge $-q$ which can be considered to lie at its centre. A point charge $+q$ placed at F where AF $= \zeta$ includes image charges $\pm qr_1/\zeta$ at A and E. As F approaches the surface, $(\zeta \to r_1)$ the charges at A cancel more and more exactly. It is as if the charge $-q$ at A had moved to E, where AE.AF $= \zeta'\zeta = r_1^2$.

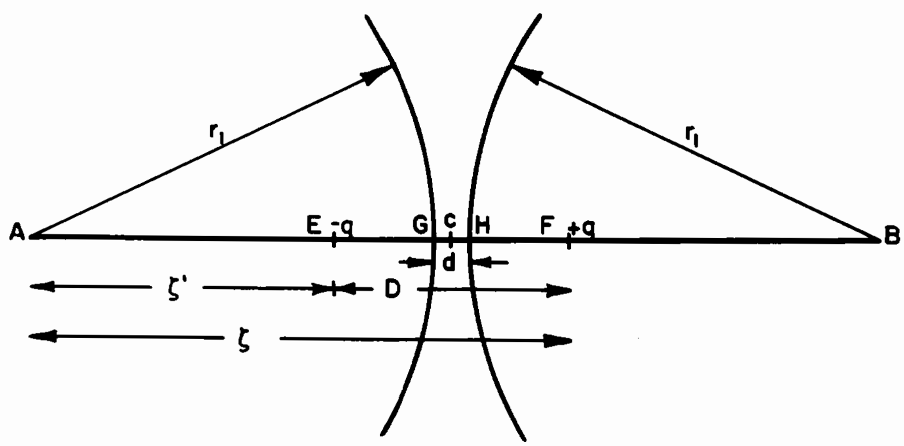

Figure 4.2 Approximate model for determining close range attraction between charged spheres. The charges $+q$ and $-q$ on the two spheres have been moved from the centres A and B to E and F. To determine their positions, it is assumed that each is the image of the other.

Then $\zeta'\zeta = r_1^2$ and $\zeta + \zeta' = 2r_1 + d$

therefore $D^2 = (\zeta - \zeta')^2 = (\zeta + \zeta')^2 - 4\zeta\zeta' = 4r_1 d + d^2 \doteq 4r_1 d$

since $d \ll 4r_1$.

acceleration of the droplets towards each other, but only acts for a limited time, of the order $2r_1/U$, which is 4.8×10^{-3} sec. Assuming the value $f = 55 \times 10^{-12}$ dyne to apply throughout this period, the distance travelled by each droplet towards the other in this time would be 4.5×10^{-4} microns, sufficient to convert only a very small proportion of encounters into collisions.

The method of arriving at this result is rather approximate. In particular, it involves the very questionable procedure of figures 4.1 and 4.2. Instead of attempting to justify the method, or to assess its limits of accuracy, an upper limit to the value of f can be found as follows. It can be said with certainty that the attraction cannot possibly exceed that between two charges $\pm q$ situated at G and H (figure 4.2), so that the maximum possible value of f for a given value of d is found by putting $f = q^2/(4\pi d^2)$. Then $f = 16.5 \times 10^{-8}$ dyne and if it acted for 4.8×10^{-3} second, each droplet would move 0.14 microns towards the other and collisions would indeed occur. Even so, the collision cross section would only have a radius of the order 0.2 microns compared to the encounter cross section which has a radius of 30 microns; the collision efficiency would be increased from 0 to about 0.5×10^{-4}.

For other radii, other values apply, but none are very sensitive functions of radius, and there seems very little chance that collision efficiencies are materially affected by the charges normally encountered on droplets in neutral warm clouds. In non-neutral clouds the charges are larger but predominantly of the same sign; they would hinder rather than help coalescence.

It is not suggested that this brief study of the influence of charge on coalescence should replace the thorough investigation that the topic deserves, but the very small calculated effects suggested that other possible causes of coalescence should be investigated.

5. CONDENSATION

5.1 Theory

Howell (1949) has described the process of condensation in ascending air. The air is cooled until water vapour condenses on to nuclei, making them into droplets; the vapour then continues to condense on to the droplets. The air becomes slightly supersaturated and a droplet gains water according to the following law:

$$\frac{S}{100} = Fr\frac{dr}{dt} + \frac{F_1}{r} - \frac{F_2}{r^3} \qquad (5.1)$$

where r = radius of droplet,

S = supersaturation in percent

F_1 is defined by Howell and takes account of the work done against surface tension,

F_2 depends on the soluble material in the nucleus,

$F = F_4 + F_5F_6$, where F_4, F_5 and F_6 relate to the transport of vapour and heat.

MacDonald (1953) claims that Howell used an incorrect value of F_2 through neglecting to consider Raoult's Law and assuming 100 percent dissociation of the electrolyte when a hygroscopic nucleus is dissolved. Had allowance been made for incomplete dissociation, the calculated relative rates at which nuclei of various sizes grow into droplets would have been considerably affected. This in turn would have left its mark on the results of all subsequent calculations of droplet size distributions. Whether this is the case or not, the size distribution of condensation nuclei is not known with any certainty so no great reliance can be placed on curves of droplet sizes derived from them.

Both difficulties are avoided by starting from the idealised fair-weather cumulus distribution, which is an approximation to observed droplet distributions. All the droplets in it are large enough for the F_2 term to be quite negligible compared to the others.

Neglecting F_2/r^3 and multiplying through by r, equation (5.1) becomes

$$\frac{S}{100} r = F r^2 \frac{dr}{dt} + F_1$$

$$= \frac{F}{4\pi\rho_s} \frac{dm_r}{dt} + F_1 \qquad (5.2)$$

where m_r = the mass of the droplet

ρ_s = density of water

Summing over all droplets in one cubic metre of air

$$\frac{S}{100} \sum_1 r = \frac{F}{4\pi\rho_s} \frac{dW}{dt} + F_1 N_1 \qquad (5.3)$$

where $\sum_1 r$ = sum of the droplet radii per m^3

N_1 = number of droplets per m^3

dW/dt = rate of increase of water content of droplets

= rate of loss of water vapour from the air.

Then

$$\frac{S}{100} = \frac{F}{4\pi\rho_s \sum_1 r} \frac{dW}{dt} + \frac{F_1}{\bar{r}} \qquad (5.4)$$

where $\bar{r} = \sum_1 r/N_1$ = mean radius, Rewriting (5.2) in the form

$$\frac{1}{4\pi\rho_s}\frac{dm_r}{dt} = \frac{1}{F}\left[\frac{S}{100}r - F_1\right]$$

and substituting from (5.4), we get

$$\frac{1}{4\pi\rho_s}\frac{dm_r}{dt} = \frac{F_1}{F}\left[\frac{r}{\bar{r}} - 1\right] + \frac{1}{4\pi\rho_s}\cdot\frac{r}{\sum_1 r}\cdot\frac{dW}{dt} \qquad (5.5)$$

5.2 Redistribution of water

Equation (5.5) shows that transfer of vapour occurs even when no overall condensation is taking place. Putting $dW/dt = 0$ we see that droplets of radius smaller than the mean, for which $r < \bar{r}$, are losing water, and those greater than the mean ($r > \bar{r}$) are gaining it. Water is diffusing (via the ambient vapour) from the smaller to the larger drops.

The cloud is unstable, in fact, but this process of redistribution is comparatively slow. Equation (5.5) was applied to the idealised fair-weather distribution using a method similar to that described in Appendix 2. Figure 5.1 shows the computed effect of a lapse of 30 minutes. The curve of water content distribution has become a little narrower, while the mean radius has increased slightly, but at such a slow rate that the effect would not be noticed in the life-time of a droplet in an active cumulus.

When dW/dt is not zero, the condensation of additional water from vapour on to the droplets is superimposed on this redistribution of liquid water. When condensation is rapid, the term $(F_1/f)(r/\bar{r} - 1)$ of equation (5.5) (which represents

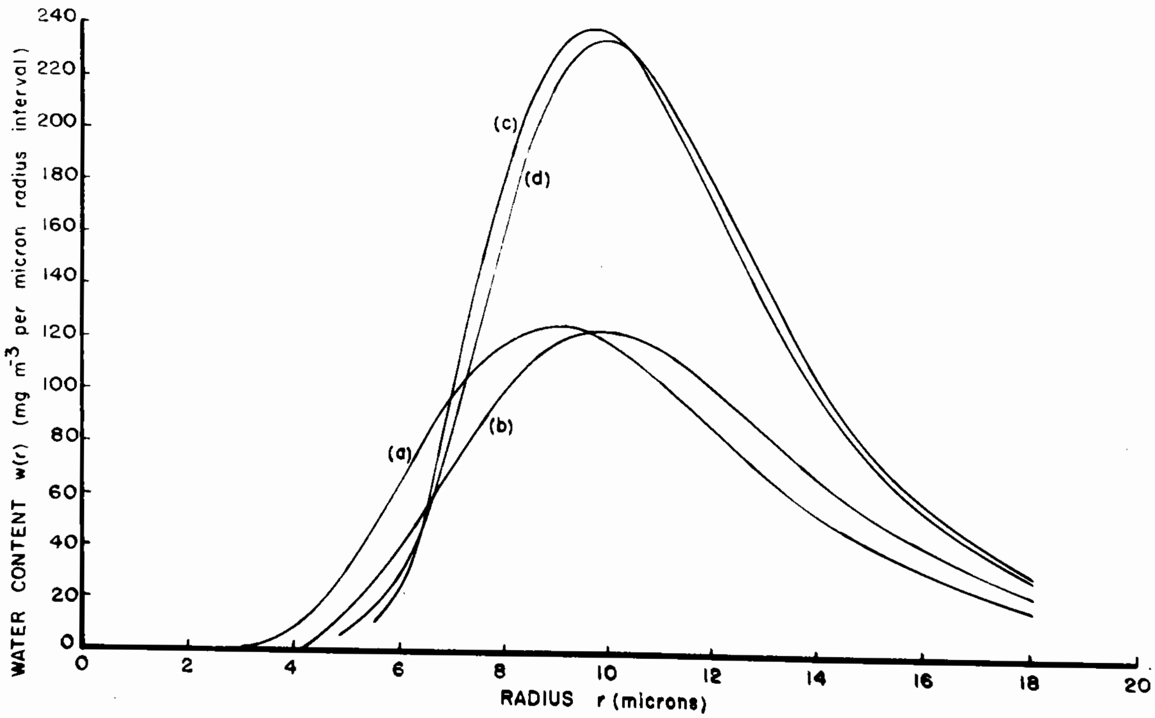

Figure 5.1 Redistribution of water through the vapour phase.
(a) Water content distribution of I.F. cloud.
(b) The distribution after 30 minutes have elapsed; the total liquid water content is unchanged but the smaller droplets have lost water by evaporation and the larger ones gained water by condensation.
Condensation of an additional 0.6 g m^{-3} on to I.F. cloud.
(c) Rapid ascent, neglecting redistribution.
(d) Slow ascent, taking 10 minutes; this corresponds to an updraft of about 1 m sec^{-1}.
(The calculations giving (c) and (d) are very approximate because the change from 1 to 1.6 g m^{-3} was made in a single step; the optimum size of step is discussed in Appendix 2. The resulting error, however, does not obscure the point at issue.)

redistribution) can be neglected in comparison with the final term. Figure 5.1 shows the effect on water content distribution due to the addition of 0.6 g m^{-3} of liquid water to the idealised distribution (1 g m^{-3} initially). In curve (c) the addition was assumed to take place rapidly so that redistribution was neglected; but curve (d) shows that even if the water is added as slowly as 1 mg m^{-3} sec^{-1} (corresponding to an updraft of only about 1 m sec^{-1}) the result is almost the same. Consequently, the redistribution term has been neglected in all subsequent calculations and equation (5.5) simplified to

$$\frac{dm_r}{dt} = \frac{r}{\sum_r r} \frac{dW}{dt} \tag{5.6}$$

The quantity dW/dt is the rate of conversion of water from the vapour to the liquid phase. The hydrostatic equation for an adiabatic ascent assumes that the vapour pressure is the equilibrium value for a flat water surface at the ambient temperature, and therefore does not apply exactly to a growing cloud. The supersaturation S does not exceed 1%, however, and varies quite slowly as the cloud develops, so the hydrostatic equation can be used with fair accuracy, or an adiabetic curve followed on a T-ϕ diagram. In short, the air does not "store" much vapour by being supersaturated.

A more serious effect is produced by entrainment of unsaturated environmental air into the updraft. It is found experimentally (Weickmann and aufm Kampe, 1953, Zaitsev, 1950) that for every metre of height above the cloud base, liquid water content W increased by about 1 mgm m^{-3}, so this has been assumed as a working value, except where a truly adiabatic ascent ~~ascent~~ without entrainment is envisaged, when the value is more like 1.4 mgm m^{-3} per metre in temperate latitudes.

5.3 Condensation alone

Figure 5.2 shows the calculated result of condensing water on to the initial idealised fair-weather distribution without any other agency at work. It can be seen that the principal effect is to "pile up" water at radii between 6 and 16 microns. Although dm/dt is proportional to r so that the largest drops receive the greatest share of the water, they have to apply it to a surface area which is proportional to r^2, making dr/dt go as r^{-1}, so that the right hand end of the distribution moves slowest. Such behaviour is quite out of keeping with the observed development of the heavy cumulus distribution. Besides, there is no way for the total number of droplets to decrease.

It is more interesting to go on to consider the action of gravity on one of these distributions. Appropriate conditions are envisaged in Scorer and Ludlam's (1953) "bubble theory". A parcel of air inside one of the bubbles would first ascend rapidly, so that the cloud droplets in it are chiefly subject to condensation. At some stage the parcel leaves the bubble and remains at approximately constant height; now gravity remains as the principal agent and coalescence takes place.

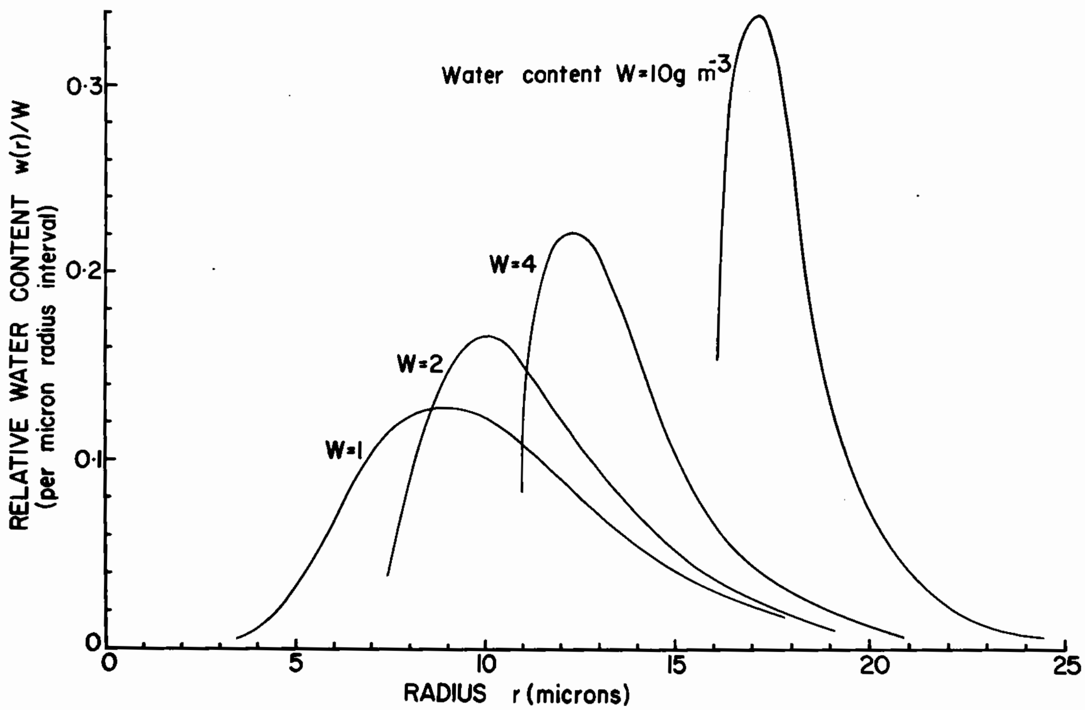

Figure 5.2 Modification of water content distribution by condensation. The curve W = 1 is for I.F. cloud: the other curves show the distribution after water is condensed on to it rapidly. All are normalised to have equal area: the peak water content $w(r)_{max}$ actually increased 26 times from W = 1 to 10 gm^{-3}.

For purposes of calculation the distribution after reaching 4 g m^{-3} was taken (corresponding to a truly adiabatic ascent from the condensation level of about 3 km in temperate latitudes). At this stage the droplets have radii up to 17 microns and the drops from 17 to 21 microns. The action of gravity in causing collisions between drop and droplets was calculated by the method of appendix 1; the result is shown in figure 5.3.

The change to a heavy cumulus type of distribution takes only about one-tenth as long as it did when gravity acted directly on I.F. cloud (compare figure 5.3 with figure 3.4). This enhanced speed is mainly due to the increase of roughly 60 percent in droplet radius brought about by the condensation beforehand. If conditions exist in the cloud which allow these processes to act in this way, we have quite a possible mechanism for bringing about the observed change in the droplet size distribution, and ultimately producing precipitation. Such conditions will be discussed again in section 8 below.

5.4 Condensation with gravity

The computation of section 5.3 neglected the action of gravity in the first part of the process, i.e. it was assumed that the condensation occurred in such a short time that gravity produced very few collisions. It might be, however, that the updraft is slow enough for gravity to play a part in modifying the droplet size distribution while condensation is

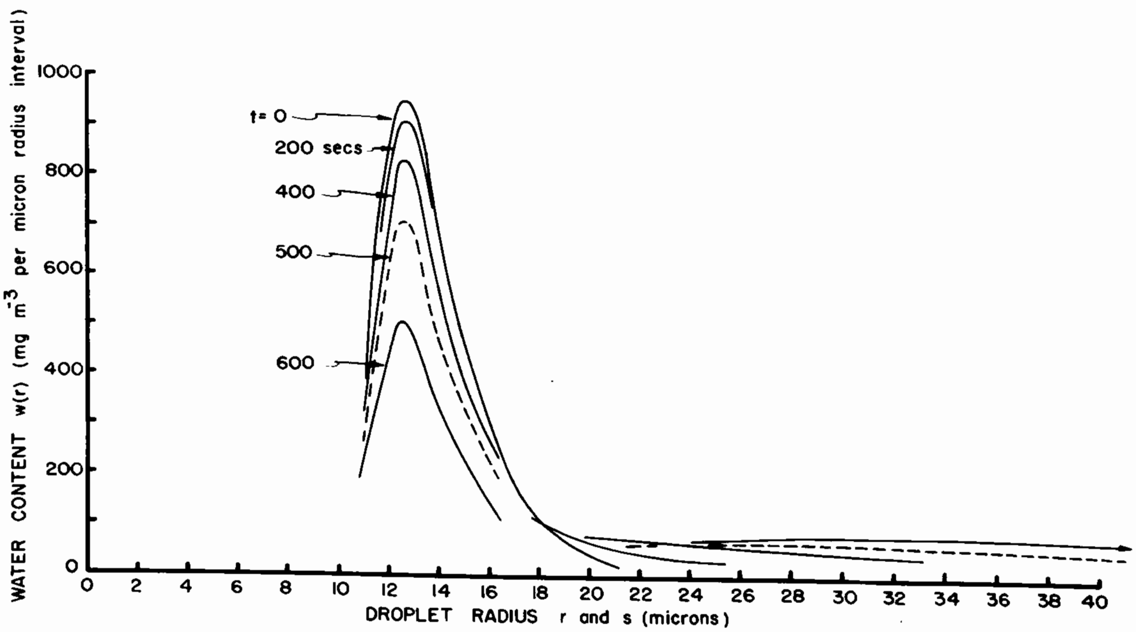

Figure 5.3 Modification of water content distribution by coalescence (after condensation). The curve t=0 is the distribution for W = 4 of figure 5.2. Droplets, whose radii in the I.F. cloud lay below 13 microns and whose radii now extend up to 17 microns, are swept up by drops above 17 microns. After 10 minutes (last curve) the largest drops reach 50 microns.

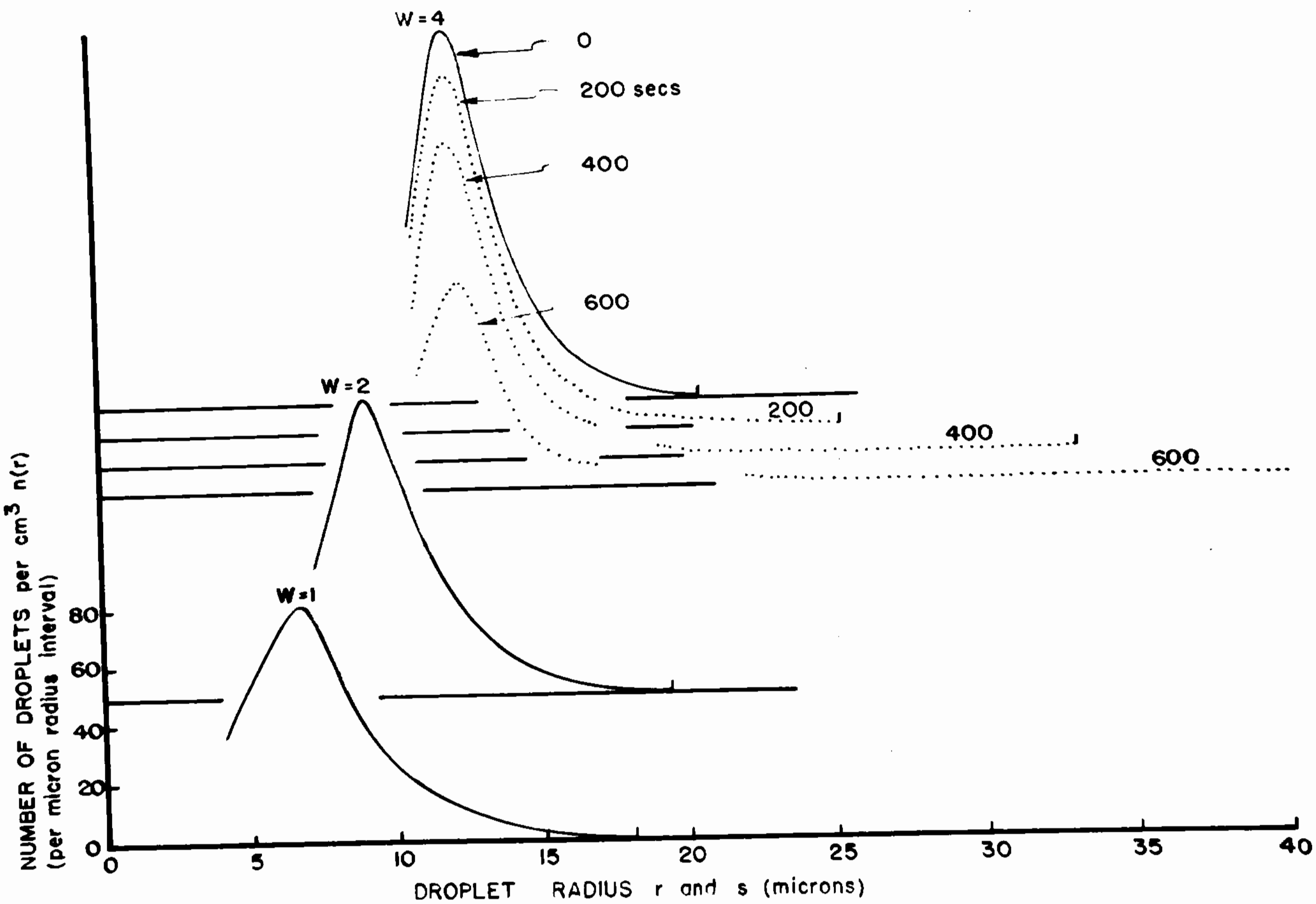

Figure 5.4 Modification of droplet number distribution by condensation, followed by coalescence.
Solid curves. Rapid ascent of parcel of I.F. cloud until water content is 4 gm^{-3}.
Dotted curves. The parcel then stays at constant height while gravity causes coalescence. The last curve extends to 50 microns. The vertical displacement is for clarity only.

still taking place.

The updraft velocity controls the ratio between the quantity of water condensed and the time elapsed at each stage. Take an arbitrary figure for this ratio of 3 mg m^{-3} per metre; it corresponds to about 2 m sec^{-1} of saturated adiabatic ascent, or about 3 m sec^{-1} allowing for entrainment of environmental air, which are not very high updraft velocities for a vigorous cumulus. The calculations of section 5.3 were repeated, but in alternate smaller steps of condensation and gravity to approximate a simultaneous action.

Figure 5.5 shows the development of the water content distribution with time. A pronounced peak develops at about 12 microns radius, just as it did without gravity (figure 5.2); in addition, some growth of the largest drops takes place. When gravity acted after condensation, however, ten minutes was sufficient time for the largest droplets to reach 50 microns (figure 5.3), whereas here they only reach 23 microns. Of course, the curves of figure 5.3 represent 4 g m^{-3} of water instead of 2.8 g m^{-3}; it may be more appropriate to compare them with the final (15 minute) curve of figure 5.5, where the water content is 3.7 g m^{-3}. Even here, the largest droplets have still only reached 30 microns radius, and the curve is clearly becoming less, rather than more, like the idealised heavy cumulus as time proceeds.

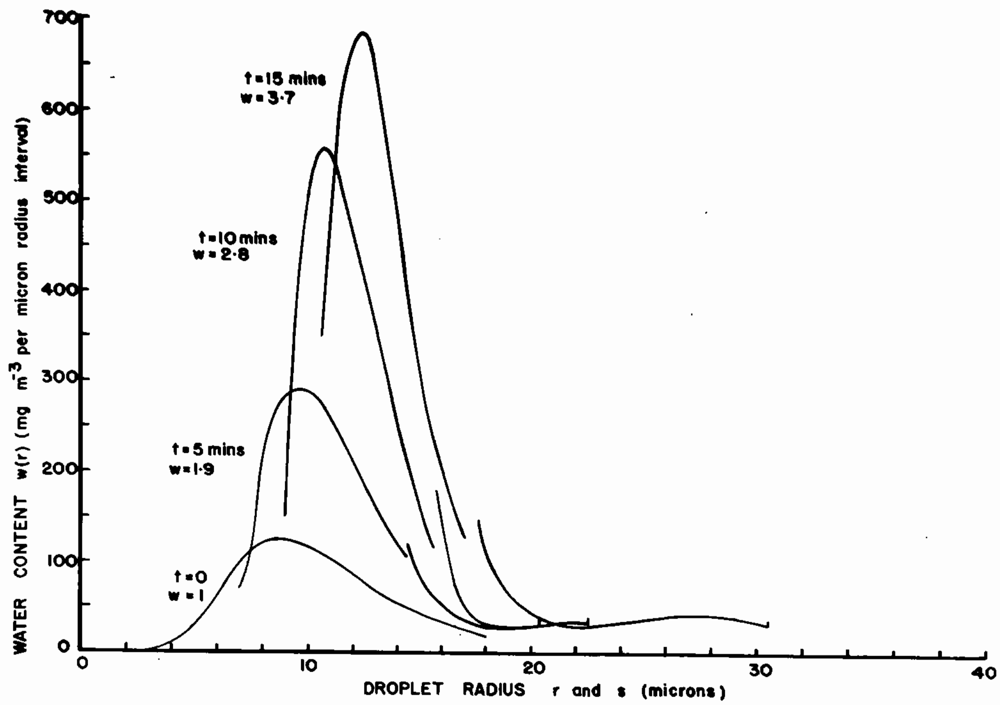

Figure 5.5 Modification of water content distribution by coalescence and condensation simultaneously. The curve $t = 0$ is for I.F. cloud. Water is added at the rate of 0.003 g m^{-3} per second (as in an updraft of about 3 m sec^{-1}, allowing for entrainment).

6. COALESCENCE BY TURBULENCE

6.1 Introduction

In the M.Sc. Thesis the theoretical foundations were laid for computing the effect of turbulence on collision rate. It was pointed out that components of motion in turbulence are approximately Gaussian so that even if the r.m.s. velocities induced by the turbulence are no greater than the terminal velocities caused by gravity, part of the time velocities are greater, (occasionally much greater), so that collisions are possible between pairs of droplets which could never collide at all with gravity. Collision rates for this case were computed.

The theory will be recapitulated in revised form. The earlier treatment considered only one-dimensional turbulence and neglected gravity; here we consider somewhat more realistic models of turbulent motion, calculate the collision rate for various combinations of drop and droplet, and use the results to compute the growth of drops.

Turbulence, for the present purpose, is an isotropic random motion, but gravity is anisotropic, since it is directed vertically. When the r.m.s. velocities induced by turbulence are much less than the velocities caused by gravity, however, the horizontal components are very unlikely to induce collisions in cases where gravity alone fails, or to increase the number noticeably where gravity succeeds. The vertical component, however, is alternately assisting and opposing gravity and it is this component, if any, which will affect the collision rates. This is the idea behind the case considered in the next sub-section where a one-dimensional random relative velocity is added to the steady relative velocity due to gravity. The results are not exact since the r.m.s. random velocity is taken equal to the steady.

When the turbulent velocities are much greater than those due to gravity, the roles are reversed. Gravity assists downward vertical velocities and hinders upward ones, but the results tend to average out. The effects of the vertical component differ little from those of the horizontal, and gravity can be ignored. This is the basis for the sub-section on three-dimensional turbulence.

6.2 One-dimensional turbulence with gravity

6.2.1. Mean efficiency. For a given drop, radius s, and droplet, radius r, in a steady gravitational field g_E, the relative velocity U, Langmuir's parameter K, and collision efficiency E have steady values which depend on s, r; call them U_1, K_1 and E_1. When the excitation is random U, K and E are also random functions of time. We define $k = U/U_1$, so that $K = kK_1$; k will be called the "reduced Langmuir parameter". Whenever the relative velocity happens to have the value it would have with gravity alone, $k = 1$.

The mean equivalent volume sweeping rate for s and r

$$Q'(s,r) = \pi (s+r)^2 \,\overline{UE} = \pi (s+r)^2 \int_0^\infty U\, E(K)\, P(U)\, dU \qquad (6.1)$$

where P(U)dU is the probability that the relative speed lies between U and U + dU. Then

$$Q'(s,r) = \pi(s+r)^2 \; U_1 \int_0^\infty k \; E(kK_1) \; P(k) \, dk \tag{6.2}$$

We can put

$$E' = \int_0^\infty k \; E(kK_1) \; P(k) \, dk \tag{6.3}$$

and call E' the mean efficiency for this particular probability distribution.

The steady relative velocity due to gravity g_E is $U_1 = (\tau_s - \tau_r) g_E$ if Stokes's Law applies. It was shown in the M.Sc. Thesis (see also Appendix 3(a)) that the contribution to relative velocity due to a fluctuating acceleration A is

$$U(t) \doteqdot (\tau_s - \tau_r) \, A(t) \tag{6.4}$$

provided the spectrum of air velocity satisfies certain conditions. (This expression is only true when Stokes's Law is obeyed, but it is shown in Appendix 3(b) that the departure from Stokes' Law does not introduce a large error). Then since A(t) has a Gaussian distribution, so has U(t); we take the r.m.s. value of A(t) equal to g_E, so the r.m.s. value of U(t) is U_1. Then

$$P(U)\,dU = \frac{1}{U_1 (2\pi)^{1/2}} \left[\exp\left\{ -\frac{(U-U_1)^2}{2U_1^2} \right\} + \exp\left\{ -\frac{(U+U_1)^2}{2U_1^2} \right\} \right] dU \tag{6.5}$$

where U now refers to relative speed rather than velocity. In reduced form

$$P(k)\,dk = (2\pi)^{-1/2} \left[\exp\{-(k-1)^2/2\} + \exp\{-(k+1)^2/2\} \right] dk \tag{6.6}$$

This probability distribution is plotted in figure 6.1 curve (c). The dashed curve (a) represents the contribution due to the first term in equation (6.6); curve (b) comes from the second term in the equation, and shows the probability that the random acceleration overcomes gravity and produces relative velocity in the reverse direction.

The function E' given by the integral (6.3) above was computed numerically for about 20 values of K_1 ranging from 0.25 to 40 and is plotted in figure 6.2. It is apparent that for any drop s and droplet r to which a value K_1 applies, E' is always somewhat greater than E so that the added turbulence is increasing the chance of collisions; moreover, collisions can occur in cases where $K_1 < 1.214$, for which collisions are not possible at all with gravity alone.

6.2.2 Growth of drop. The mean equivalent volume sweeping rate

$$Q'(s,r) = \pi(s+r)^2 U_1 E' \tag{6.7}$$

from equations (6.2) and (6.3). Figure 6.3 shows that it is always larger than Q(s,r) in figure 3.1 (this follows from the fact that $E' > E$). The most noticeable difference is for the smallest droplets ($r = 4$), but more important is the fact that at $s = 15$ microns appreciable collision rates occur for most droplet sizes.

Figure 6.4 shows the relative contribution of droplets of various sizes to the growth of a drop falling through I.F. cloud. Figure 6.5 shows how the drop grows with time; by

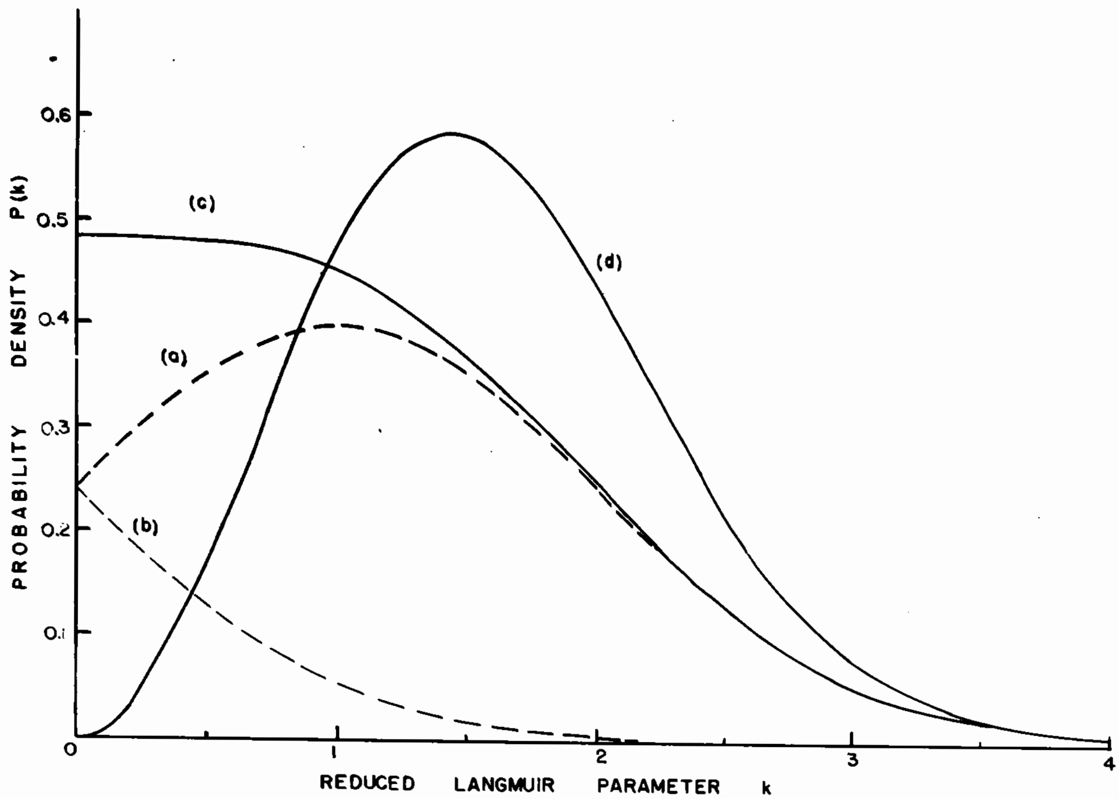

Figure 6.1 Probability density distributions of acceleration in turbulent air.
(a), (b), (c). One-dimensional turbulence parallel to gravity, $(\overline{A^2})^{1/2} = g_E$; (a) probability distribution for resultant accelerations in the same sense as gravity; (b) p.d. for resultant accelerations in the opposite direction; (c) combined probability distribution for resultant acceleration, regardless of sense. The flatness of the curve near $k = 0$ is a fortuitous result of making $(\overline{A^2})^{1/2} = g_E$.
(d) Three-dimensional turbulence neglecting gravity, and neglecting correlation between components (Rayleigh distribution).

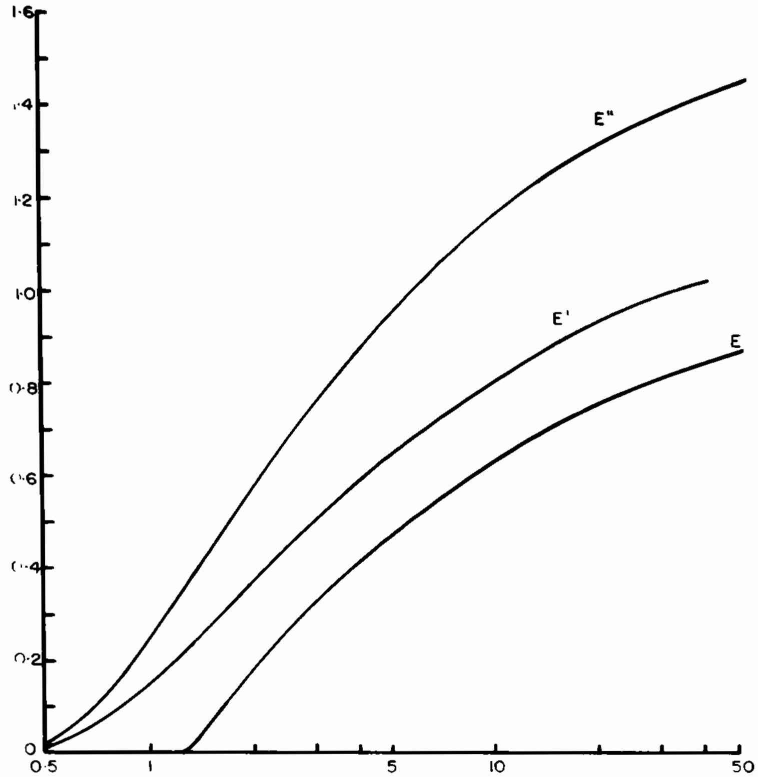

Figure 6.2 Collision efficiency, and mean efficiencies.
Curve E. Collision efficiency versus Langmuir's parameter K. As $K \to \infty$, $E \to 1$.
Curve E'. One-dimensional turbulence, $(\overline{A^2})^{1/2} = g_E$: mean efficiency versus K_1, the value which K has when acceleration = g_E. As $K_1 \to \infty$, $E' \to 1.17$.
Curve E''. Three-dimensional turbulence, $(\overline{A^2})^{1/2} = 2g_E\sqrt{3}$: mean efficiency versus K_2, the value which K has when acceleration = $2g_E$. As $K_2 \to \infty$, $E'' \to 1.60$.

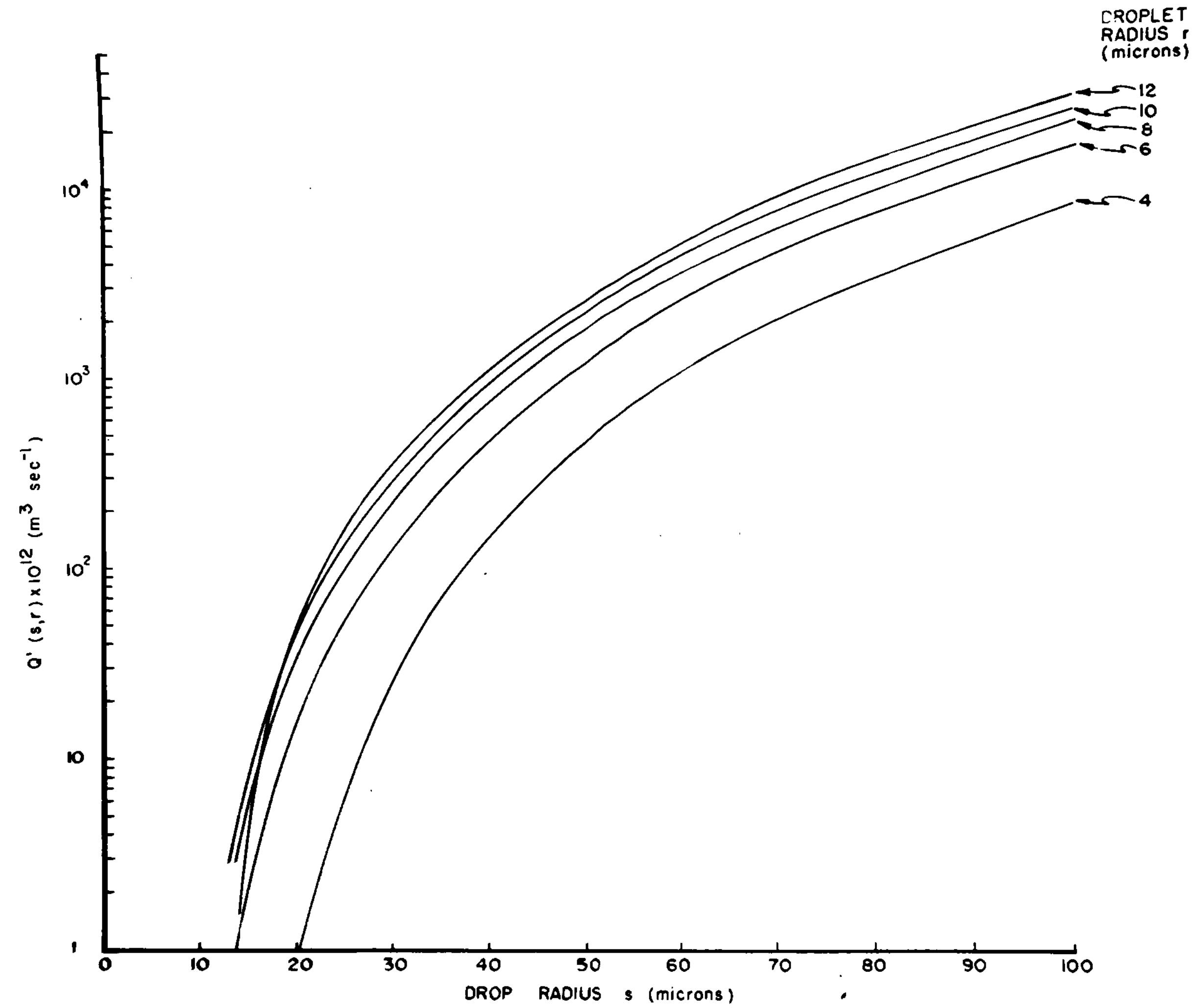

Figure 6.3 Mean equivalent volume sweeping rate (one-dimensional turbulence with gravity). The quantity Q'(s,r) versus drop radius s, for the droplet radius r shown on curve, in conditions specified by figure 6.1(c).

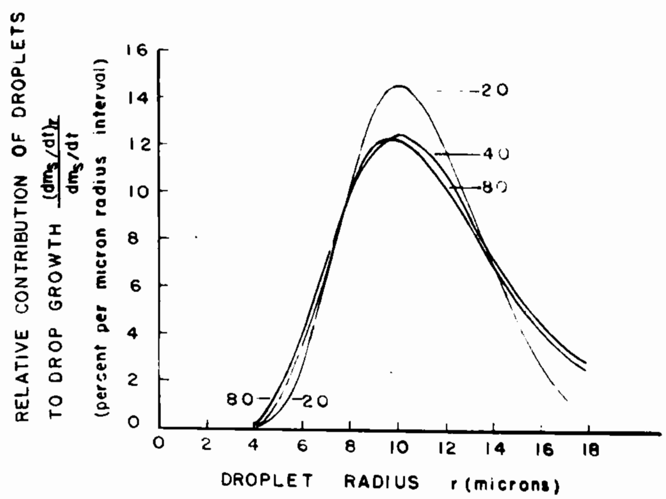

Figure 6.4 Relative contributions of droplets to growth of drop (turbulence with gravity). Percentage of dm_s/dt contributed by droplets of radius r (per micron) versus r, as drop of radius s falls by gravity through I.F. cloud which is in turbulent motion.

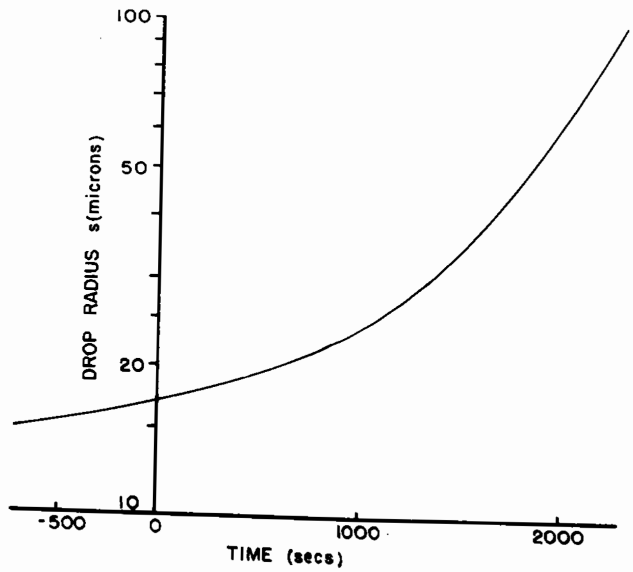

Figure 6.5 Growth of drop by coalescence (turbulence with gravity). Drop radius versus time, as the drop falls by gravity through I.F. cloud in turbulent motion.

comparison with figure 3.3 for gravity alone, it appears that the addition of turbulence has speeded up growth, particularly in the early stages. However, it still takes over 40 minutes for the drop to grow from 17 to 100 microns. This is rather a long time on the time-scale of cumulus development.

6.2.3 Modification of droplet-size distribution. The progressive change in the distribution of I.F. cloud with time were calculated using the mean equivalent volume sweeping rate Q'(s,r) just discussed. The technique introduced in section 3.4 and described in Appendix 1(b) was used: the results are shown in figure 6.6.

The last curve shown looks very promising as a potential heavy cumulus distribution. The depletion of small droplets is accompanied by an extension of the distribution out to 40 microns, which could obviously continue with time. Figure 6.7 shows five of the same curves replotted as droplet-number distributions. They resemble the measured curves of Zaitsev (1950) at successive levels in a cumulus.

Both 6.6 and 6.7, however, represent the result of an hour's action by turbulence and gravity combined. The growing of large cloud drops, which is only part of the overall transition from young cumulus to rain-cloud, often takes much less time than this. Still greater speed is required.

6.3 Three-dimensional turbulence.

In continuing the investigation to greater intensities of turbulence, the effect of gravity is neglected. The random

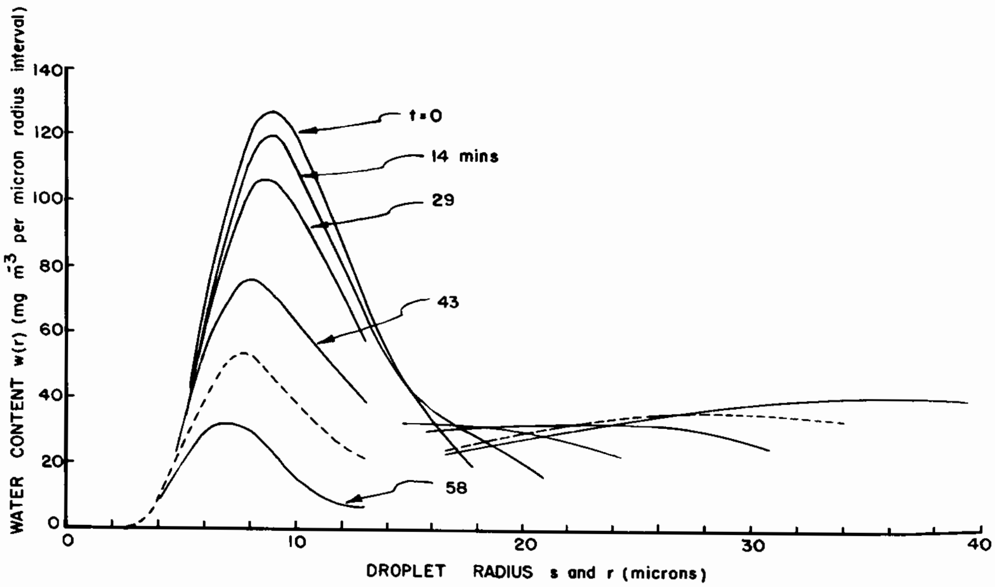

Figure 6.6 Modification of water content distribution by coalescence (turbulence with gravity). The curve t = 0 is for I.F. cloud: the curves for later times show the result of one-dimensional turbulence acting with gravity. Compare the time scale with that of figure 3.4.

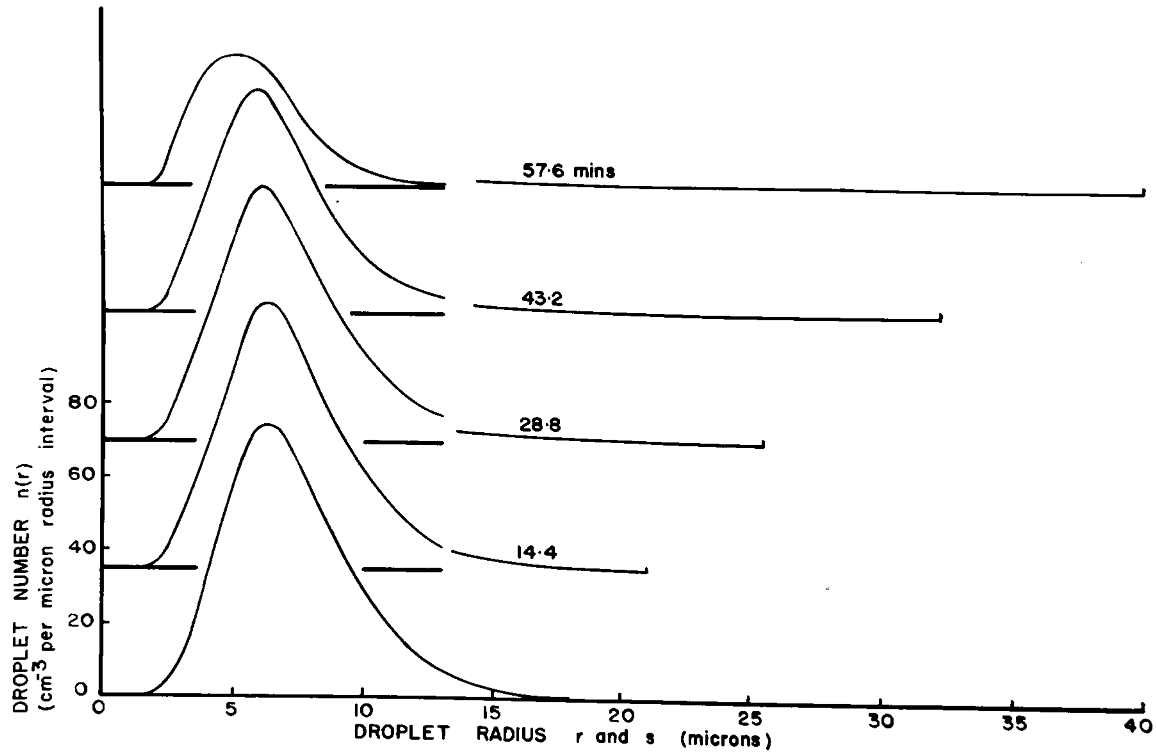

Figure 6.7 Modification of droplet number distribution by coalescence (turbulence with gravity). The lowest curve is for I.F. cloud. The vertical displacement is for clarity only.

acceleration is assumed to be made up of three independent components which have Gaussian distributions with equal r.m.s. values. In turbulent motion the three components are not independent, and the correlation between them affects the resultant probability distribution. In Appendix 3(c) reasons are given for supposing the correlation to be negligible for the present purpose; then the probability distribution of the magnitude of accelerations becomes simply a Rayleigh distribution.

We assign arbitrarily the value $2g_E$ to the r.m.s. linear acceleration in each direction. Whenever the acceleration happens to have this value, the relative velocity between drop s and droplet r is U_2, the relative terminal velocity it would have in a steady gravitational field $2g_E$, (provided turbulence has a suitable spectrum). The acceleration in three dimensions, then, has a Rayleigh distribution with an r.m.s. value $\sqrt{3}.2g_E$, an although Stokes' Law is not obeyed, we assume that the relative speed U(t) has a Rayleigh distribution with r.m.s. $\sqrt{3}.U_2$.

The mean equivalent volume sweeping rate for three-dimensional turbulence

$$Q''(s,r) = \pi(s+r)^2 U_2 E'' \qquad (6.8)$$

where U_2 = relative terminal velocity that a drop s and droplet r would have in a steady field $2g_E$.

The need for using U_2 instead of U_1 is discussed in Appendix

3(b). The mean efficiency

$$E'' = \int_0^\infty k\, E(kK_2)\, P(k)\, dk \tag{6.9}$$

where $K_2 = U_2 \tau_r/s$.

The probability distribution used is the Rayleigh distribution

$$P(k)\,dk = \left(\frac{2}{\pi}\right)^{1/2} k^2 \exp\{-k^2/2\}\, dk \tag{6.10}$$

It is shown in figure 6.1 as curve (d).

The mean efficiency E" was calculated for 21 values of K_2 from 0.5 to 50 and is plotted in figure 6.2; the curve lies above those for E and E' everywhere. Moreover, this presentation does not do justice to the enhanced coalescing power of the new turbulence; for a given s and r, the value of K_2 is always nearly twice that of K_1, giving rise to a value of E" several times greater than E'. For $s = 30$ and $r = 10$ microns, for example, $U_1 = 9.6$ cm sec^{-1} and $U_2 =$ 18.6 cm sec^{-1}. Then $K_1 = 4.12$ and $K_2 = 8.0$ giving $E' = 0.60$ and $E'' = 1.10$; the product $U_1E' = 5.8$ cm sec^{-1} while $U_2E'' = 20.5$ cm sec^{-1}.

The mean equivalent volume sweeping rate Q"(s,r) is seen in figure 6.8 to be similar in behaviour to Q'(s,r) for one-dimensional turbulence (figure 6.3) but several times as great everywhere. As a result, the process of growth of a drop is similar in character (compare figure 6.9 with 6.4) but more rapid (compare 6.10 with 6.5); it takes $10\frac{1}{2}$ minutes for a drop to grow from 17 to 100 microns instead of 42 minutes. It appears that three-dimensional turbulence of

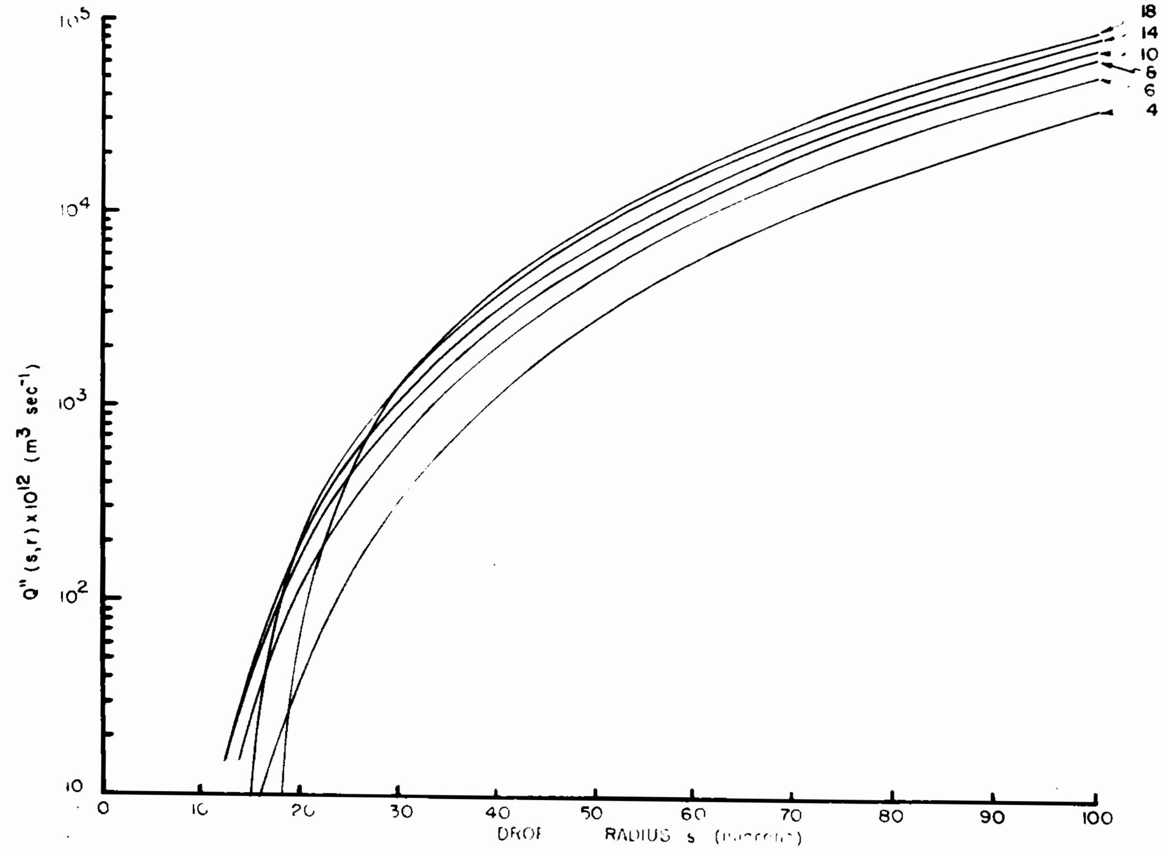

Figure 6.8 Mean equivalent volume sweeping rate (three-dimensional turbulence). The quantity Q"(s,r) versus drop radius s, for the droplet radius r shown on curve, in conditions specified by figure 6.1 (d), with $(\overline{A^2})^{\frac{1}{2}} = 2.g_E\sqrt{3}$. Note the shift in vertical ordinate from figure 6.3.

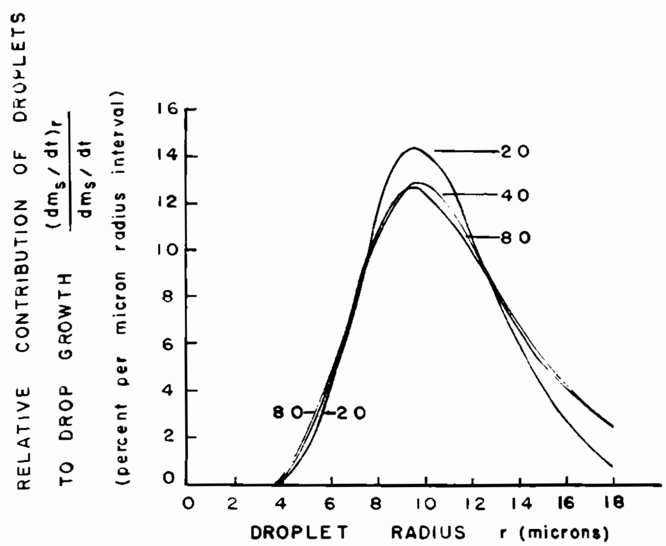

Figure 6.9 Relative contributions of droplets to growth of drop (three-dimensional turbulence). Percentage of dm_s/dt contributed by droplets of radius r (per micron) versus r, due to turbulent motion of cloud.

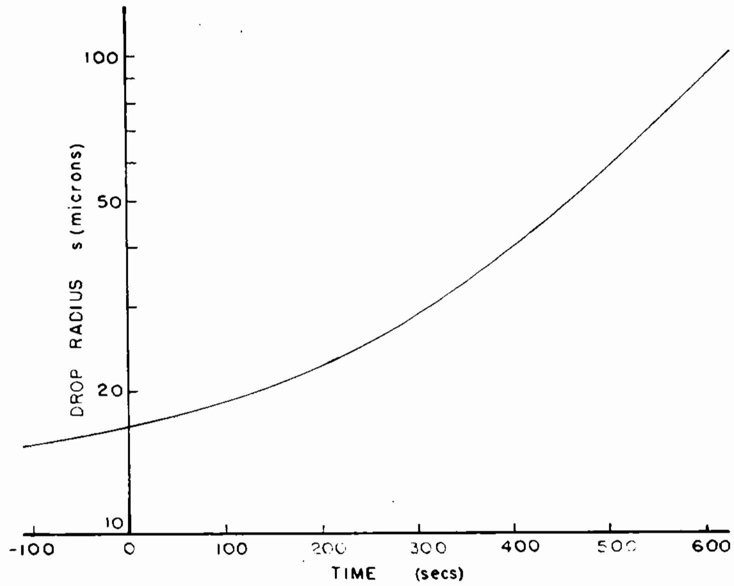

Figure 6.10 Growth of drop by coalescence (three-dimensional turbulence). Drop radius versus time, while the cloud is in turbulent motion. Note change of time scale from figure 6.5.

this intensity would be a potent mechanism in a developing cumulus.

The action of this turbulence on the complete water-content distribution (figure 6.11) is to extend it up to 37 microns in 12 minutes. The result does not resemble a heavy cumulus distribution so closely as figure 6.6: it seems that all the drops from (originally) 13 to 18 microns made rapid progress simultaneously, and exhausted the supply of droplets too soon. Perhaps the artificial division into drops that grow and droplets that disappear is no longer tolerable.

When these results are replotted as number distributions, they appear to meet the requirements. It is not really possible to decide for or against turbulence as the principal mechanism for maturing cumulus merely by matching curves. It is necessary to know what intensity of turbulence can actually be expected in clouds; some of the evidence is examined in the next section.

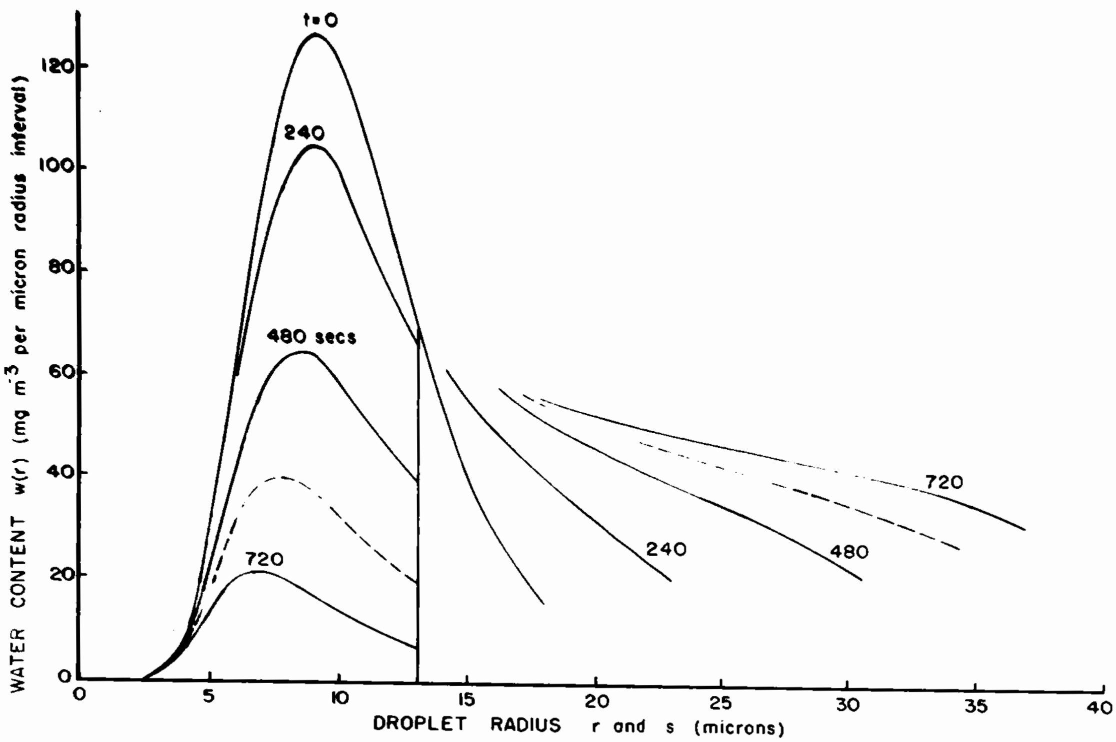

Figure 6.11 Modification of water content distribution by coalescence (three-dimensional turbulence). The curve $t \approx 0$ is for I.F. cloud: the curves for later times show the effect of turbulent motion. Compare the time scale with those of figures 6.6 and 3.4.

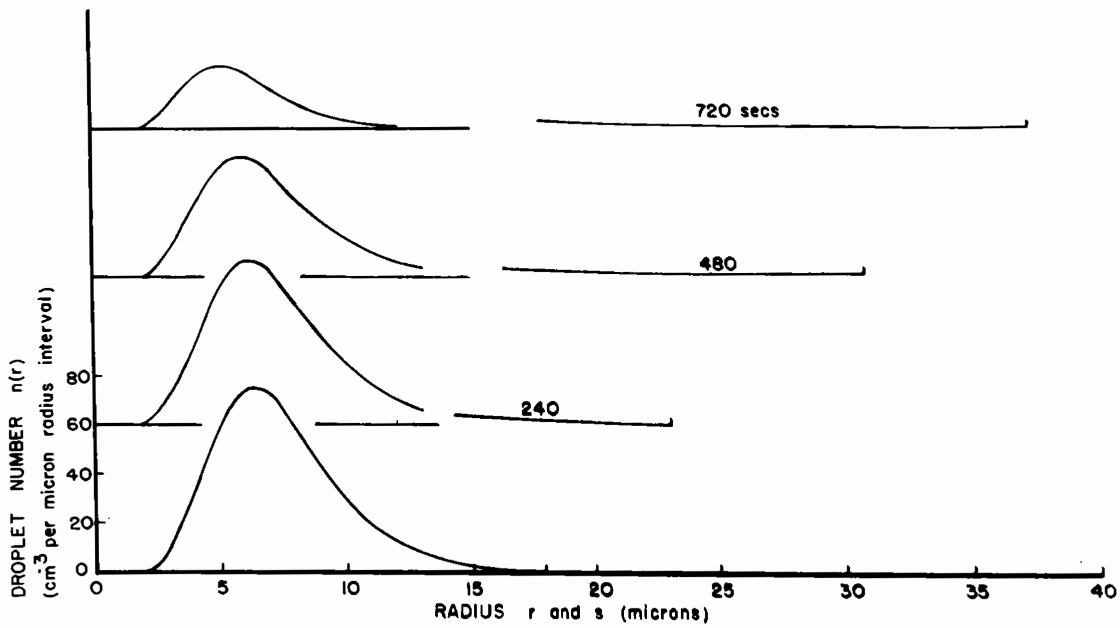

Figure 6.12 Modification of droplet number distribution by coalscence (three-dimensional turbulence). The lowest curve is for I.F. cloud. The vertical displacement is for clarity only.

7. INTENSITY OF TURBULENCE

7.1 Theory of homogeneous turbulence. The present-day theory of turbulence arises from the work of G.I. Taylor, Kolmogoroff, Heisenberg, Batchelor and others, and is presented by Batchelor in his 1953 book. This theory predicts that when air is set in motion at a very large Reynolds number R, a spectrum of eddies results which extends from the largest eddies that are produced directly by the outside source of energy, down to very small eddies which are dissipated by viscosity. The ratio of the largest to the smallest eddy diameters is about $R^{3/4}$; the eddies which lie between the two extremes are said to form the inertial sub-range, and their spectrum (i.e. the curve of energy versus wave-number) always follows a universal law. The intensity depends only on the rate at which energy is being absorbed by the turbulence, ε.

The Reynolds number R in an active cumulus cloud is of order 10^7 and this is almost certainly sufficient for the inertial sub-range to have the predicted properties; eddy sizes extend from hundred of metres to roughly 1 mm. Under these conditions a simple formula of Batchelor (1951) is applicable; it is

$$\overline{A^2} = \frac{1}{\rho^2}\overline{(\mathrm{grad}\ p)^2} = 3\nu^{-1/2}\varepsilon^{3/2} I \qquad (7.1)$$

where $\overline{A^2}$ = mean square acceleration

ρ = density

p = pressure

ν = kinematic viscosity

ε = rate of dissipation of energy by turbulence,

and I is a number whose value is not known with certainty, but is within a few tenths of 1.3.

Batchelor cites experiments by Simmons and Collis which, though very limited in scope, give the formula some verification .

7.2 Estimates of intensity of turbulence. To find the acceleration we have to estimate ε , the rate of absorption of energy by the turbulence. It is given by

$$\varepsilon = \frac{3}{2} A \frac{\left(\overline{u^2}\right)^{3/2}}{L_p} \tag{7.2}$$

where $\overline{u^2}$ = mean square velocity component in one dimension,

L_p = longitudinal integral scale,

and A is a number which, from Batchelor and Townsend's (1948) experiments is about 1.1. (See Batchelor (1953) fig. 6.1.)

Experimental measurements of $\overline{u^2}$ inside clouds are not available, but the results of instrumented aircraft flights have been published by Byers and Braham (1949) and by Malkus (1954). To make use of them we adopt the "cell" model used by Byers and Braham and assume:

1. The updraft structure can be identified with the largest eddies.

2. The updrafts account for most of the mean square velocity.

3. Although the updraft structure is not isotropic, the eddies in the inertial sub-range are isotropic, and the laws of transfer of energy still apply.

Braham (1952) gives results of the Thunderstorm Project. It was found that the median width for a singly updraft in a thunderstorm was 5,000 ft, and the overall width when two updrafts were flown through in succession had a median value of 11,000 ft. This suggests a periodic updraft structure of "wavelength" 6,000 ft or 1830 m, a wavenumber $K_p = 2\pi/1830\ m^{-1}$ and a longitudinal integral scale $L_p = \frac{3\pi}{4} K_p^{-1} = 686$ m. (See Batchelor (1953) p.105). The median updraft velocity is 22 ft sec^{-1} or 6.7 m sec^{-1}, which is taken to be the peak to peak variation in updraft along a line: the mean square vertical velocity, then, is $(6.7)^2/8$. The quantity $\overline{u^2}$ is defined as the mean square of one of the components in <u>isotropic</u> turbulence; since the updrafts are anisotropic, having negligible horizontal components, the mean square vertical velocity is taken to equal $3\overline{u^2}$ so that $\overline{u^2} = (6.7)^2/24 = 1.87\ m^2\ sec^{-2}$. Table 7.1 lists the resulting values of ε and $(\overline{A^2})^{\frac{1}{2}}$; the turbulent acceleration is quite negligible relative to gravity.

A detailed study by Malkus (1954) of two fair-weather clouds gave updraft velocities of about 3 m sec^{-1} and widths of 500 m. Here again the calculated turbulent acceleration is negligible.

Byers and Braham (1949) have published data on gusts. From the description these appear to be isotropic eddies derived from the updrafts; only the vertical component is measured (the two horizontal components have properties like the vertical), and upward and downward velocities are both encountered. Using median values, $3\frac{1}{2}$ gusts per 3,000 ft are encountered, and assuming they act alternately upward and downward, a wavelength of 1700 ft is obtained, giving L_p 197 m. The maximum velocity of each run of 3,000 ft was read, and the median of all runs is 6 ft sec^{-1} or 1.83 m sec^{-1}, giving $\overline{u^2} = \frac{1}{2}(1.83)^2 = 1.67\ m^2\ sec^{-2}$. The acceleration, given in Table 7.1, is still considerably less than gravity.

It seems surprising that the same series of flights can give two values for ε which differ by a factor 3, since the whole turbulence theory rests on the belief that ε should be independent of the size of eddy. However, it is quite possible that energy is supplied not only to the largest eddies (updrafts) but also directly to the smaller eddies measured as gusts. These smaller eddies are active in entraining outside air, and when a parcel of dry air is brought into cloud-filled air, it will become chilled and sink. A multitude of such local producers of kinetic energy would make ε increase with decreasing eddy size. It is the smallest eddies, where ε will be greater, that contribute most to the mean square acceleration $\overline{A^2}$, so that estimates of ε made at larger eddy sizes would have to be regarded as lower limits for this purpose.

It is also quite possible that the methods by which $\overline{u^2}$ and L_p have been arrived at are themselves erroneous to this extent.

<u>7.3 Checks of the estimates.</u> Estimates of turbulent energy can be checked in at least three ways for physical realism. (1) The rate of absorption of energy ε cannot exceed the available rate of supply from thermodynamic sources. (2) The pressure fluctuations must be less than atmospheric pressure. (3) The intensity must not be sufficient to radiate an audible sound.

Each of these tests sets a maximum value to the intensity, but it turns out that all are satisfied too easily to influence the estimated intensity of turbulence, except possibly the last.

<u>7.3.1 Energy supply.</u> Braham (1952) estimates that a single thunderstorm cell contains 2×10^{11} kg of air, and that during its lifetime, (say 30 minutes), it is supplied with thermal energy from the latent heat of 5.3×10^{8} kg of water. The average rate at which energy is supplied, then, is 3.3×10^{4} cm^2 sec^{-3} throughout the cell. It is clear from Table 7.1 that the loss of energy by turbulence is only a small part of

this figure, and that the foregoing estimates certainly cannot be contradicted for lack of a sufficient energy supply.

7.3.2 Pressure fluctuations. The absolute pressure cannot ever, in any place, become negative and it does not seem physically likely that it would approach zero closely. At any rate, the theory of turbulence is based, to first order, on incompressibility and if it predicted an r.m.s. pressure fluctuation comparable with the mean pressure it would clearly have become inapplicable.

Batchelor (1951) showed that for large Reynold numbers the mean square pressure fluctuation

$$\overline{p^2} = 0.34\, \rho^2 (\overline{u^2})^2.$$

Putting $\overline{u^2} = 10\ m^2 sec^{-2}$ as an extreme case, we find $\overline{p^2} =$ $3.100\ g^2\ cm^{-2}\ sec^{-4}$ or an r.m.s. fluctuation of about 6×10^{-5} atmospheres.

7.3.3 Audibility. Clouds have not been observed to radiate audible sound by virtue of the motion of the air in them. Dr. Heinz Lettau reports (in conversation) from personal experience of flights in free balloons that it is completely silent even in the heart of a cumulus cloud.

Proudman (1952) has found the energy radiated from decaying isotropic turbulence per unit mass

$$P = \alpha \varepsilon M^5 \quad \text{where} \quad M^2 = \overline{u^2}/c^2$$

where α is a numerical constant
ε is the rate of dissipation
M is the r.m.s. Mach number.

He predicts that the same result will apply for non-decaying turbulence if ε is taken to be the rate at which energy is supplied from an external source; α will be between 10 and 100.

The intensity at a point inside the turbulence due to a spherical shell of turbulent air, radius r, thickness dr, centred on the point is

$$dI = \frac{P\rho}{2}\, dr \int_0^{\pi/2} \cos\theta \sin\theta \, d\theta$$

$$= \frac{P\rho}{2}\, dr$$

If the cloud is spherical, radius r_o, and the observer at the centre, the intensity due to the whole cloud is $I = \frac{P\rho}{4}\, r_o$

For an extreme case take $M = 10^{-2}$ (so that $u^2 =$ 11 m^2 sec^{-2}) and $\varepsilon = 10^4$ cm^2 sec^{-3} for the smaller eddies. Then P lies between 10^{-5} and 10^{-4} cm^2 sec^{-3}. If the turbulent region has a radius $r_o = 1$ km then the intensity I at the centre is 2.4×10^{-4} to 2.4×10^{-3} erg sec^{-1} cm^{-2} or 2.4×10^{-11} to 2.4×10^{-10} watts cm^{-2}. The limit of audibility for a sensitive observer at 1000 c/s is 10^{-16} watt cm^{-2}, but the spectrum of turbulence does not reach this frequency. The eddies of highest frequency are of order $\eta = \nu^{3/4}\, \varepsilon^{-1/4}$ in length and $v = \nu^{1/4}\, \varepsilon^{1/4}$ in velocity, giving a pulsatance $\omega = v/\eta = \nu^{-1/2}\, \varepsilon^{1/2} =$ 424 sec^{-1} or 67 c/s. If all the sound were concentrated at this frequency (instead of being spread over a band from there donwards), it could be up to 9 db above the threshold intensity of 3×10^{-11} watt cm^{-2} for an average observer. (Steinberg, Montgomery, and Gardner, 1940).

It is unlikely, however, that any observer has been in the centre of a growing cumulus in favourable conditions of audibility at the stage where turbulence has reached a peak but precipitation has not yet begun to interfere with observations.

It may seem paradoxical that air can have an alternating acceleration equal to that in extremely powerful sound wave without producing audible sound. By way of illustration, consider a shaft rotating at 6000 r.p.m. in air. It does not radiate sound, although a small parcel of air carried round by it is performing a motion which has a horizontal sinusoidal component at 100 c/s and a peak to peak amplitude equal to the diameter of the shaft. The shaft produces a shearing movement, while the motion of a lpudspeaker diaphragm produces compression an rarefaction; in turbulence shear predominates.

To sum up, the available experimental data yields values for intensity which are much too small for turbulence to play a significant part in coalescence, but the data itself is not well suited to this purpose.

Table 7.1

	$\overline{u^2}$ $m^2\ sec^{-2}$	L_p m	R	ε $cm^2\ sec^{-3}$	$\overline{A^2}$ $cm^2\ sec^{-4}$	$(\overline{A^2})^{1/2}/g_E$
Braham (Thunderstorm Project)						
updr.	1.87	686	5.2×10^7	61.6	4,450	0.068
gusts	1.67	197	1.4×10^7	181	25,900	0.16
Malkus (Trade Cumulus)						
	1	375	2.1×10^7	44	2,690	0.053

8. DISCUSSION

8.1 Survey of mechanisms

The largest droplets normally found in a fair-weather cumulus could grow, under the action of gravity alone, to drizzle-drop size, but it would take more than an hour, and the whole process of rain formation in cumulus usually takes less, sometimes very much less, than one hour.

Woodcock (1952) has shown that the atmosphere contains giant salt nuclei which, in the condition of slight super-saturation in cumulus, might grow to say 30 microns radius quite rapidly and then continue to grow by coalescence to 100 microns. The concentration of such nuclei may well be low enough that the droplets have escaped detection in the samples so far collected in fair-weather cumuli, and yet be high enough to account for the raindrops which they eventually become. (The total volume of cloud-filled air sampled by Weickmann and aufm Kampe in fair-weather cumuli appears to have been of the order 10^{-5} m^3, while the concentration of raindrops (even while they still have small terminal velocities), and therefore of giant nuclei, would probably be not more than 10^4 per m^3.) On the other hand, these "giant" droplets would also escape detection in heavy cumulus clouds; giant nuclei cannot then account for the populations of droplets between 20 and 100 microns found in every one of the samples. It is possible that the droplets which formed from giant nuclei do indeed grow to raindrop size by gravity-induced coalescence, but it is obvious from figures 3.4 and 3.5 that gravity alone would not convert a typical fair-weather to a heavy cumulus distribution in a reasonable time, and whatever mechanism is responsible for this conversion is also a potent precipitation mechanism.

The chief cause of the failure of gravity to induce collisions is the lack of sufficiently violent encounters. The results of section 6 are summarised here in figure 8,1, which shows the effect of introducing turbulence. The graph takes the form of elapsed time required for a drop to grow from any given radius to 100 microns. A turbulent acceleration comparable with gravity shortens the times (curve TG) but not very much; increasing the acceleration by a factor 2 would bring about sufficiently rapid growth to be a satisfactory precipitation mechanism. With the smaller intensity the droplet size distributions change in a manner reasonably well in accordance with the observations, but rather slowly (figures 6.6 and 6.7). For the increased intensity the curves (figures 6.11 and 6.12) become rather too unrealistic, possibly because the artificial boundary between drops and droplets was at an unsuitable position, but the change is certainly rapid enough.

A turbulent acceleration greater than some critical value which lies between 1.7 and $3\frac{1}{2}$ times gravity, then, would

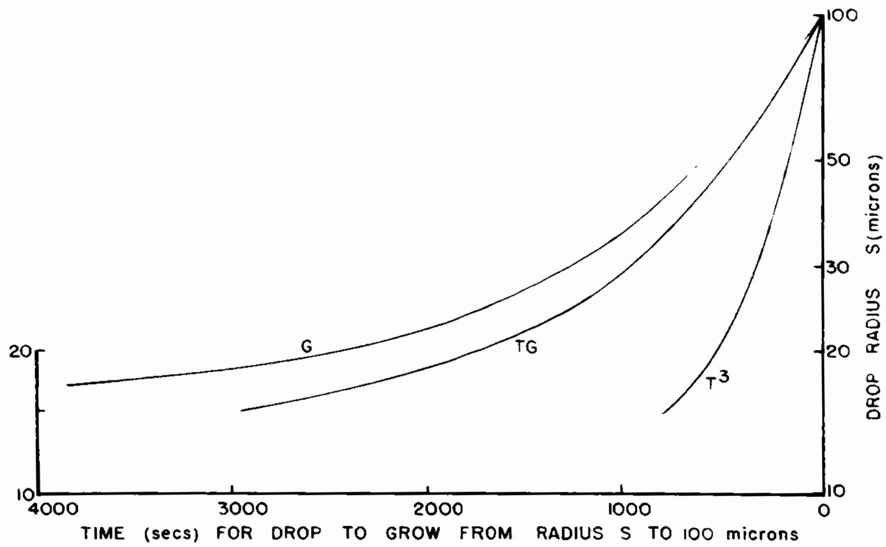

Figure 8.1 Growth of drop by coalescence (effect of intro-
ducing turbulence). Drop radius s versus time required for
drop to grow from radius s to 100 microns.
Curve G: Gravity alone. (Same as 3.3)
Curve TG: One-dimensional turbulence with gravity. (As 6.5)
Curve T^3: Three-dimensional turbulence, $(\overline{A^2})^{\frac{1}{2}} = 2g_E\sqrt{3}$ (As 6.10)

provide the precipitation mechanism sought for, but present indications are, from measurements of the motions of aircraft, that such accelerations are unlikely to occur. The extraction of this result from the data is difficult, and very approximate; in particular, median values of gust velocities were used, though occasional gust velocities several times greater had been measured. Indeed, there may be highly turbulent regions in a growing cumulus which were missed altogether by the aircraft. (Another possibility was mentioned in section 7.2.) Clearly, further, more suitable experimental data are required before reaching a final verdict, but for the present turbulence could only be accepted as an explanation if no alternative presented itself.

The cloud is convective, and in the ascending parts of it all the droplets grow by condensation. They then become suitable material for drops to feed on by coalescence. Figure 8.2 gives the life-history of a parcel of air inside a "bubble" (the element of convection described by Scorer and Ludlam, 1953). The bubble ascends, the droplet radii increasing continually (solid curves). The top surface of the bubble has been worn away during the journey, until the parcel under consideration is also dragged off and forms part of the "wake". It lies at a more or less constant height, while gravity gets to work on the droplets. In the next ten minutes the distribution changes to something rather

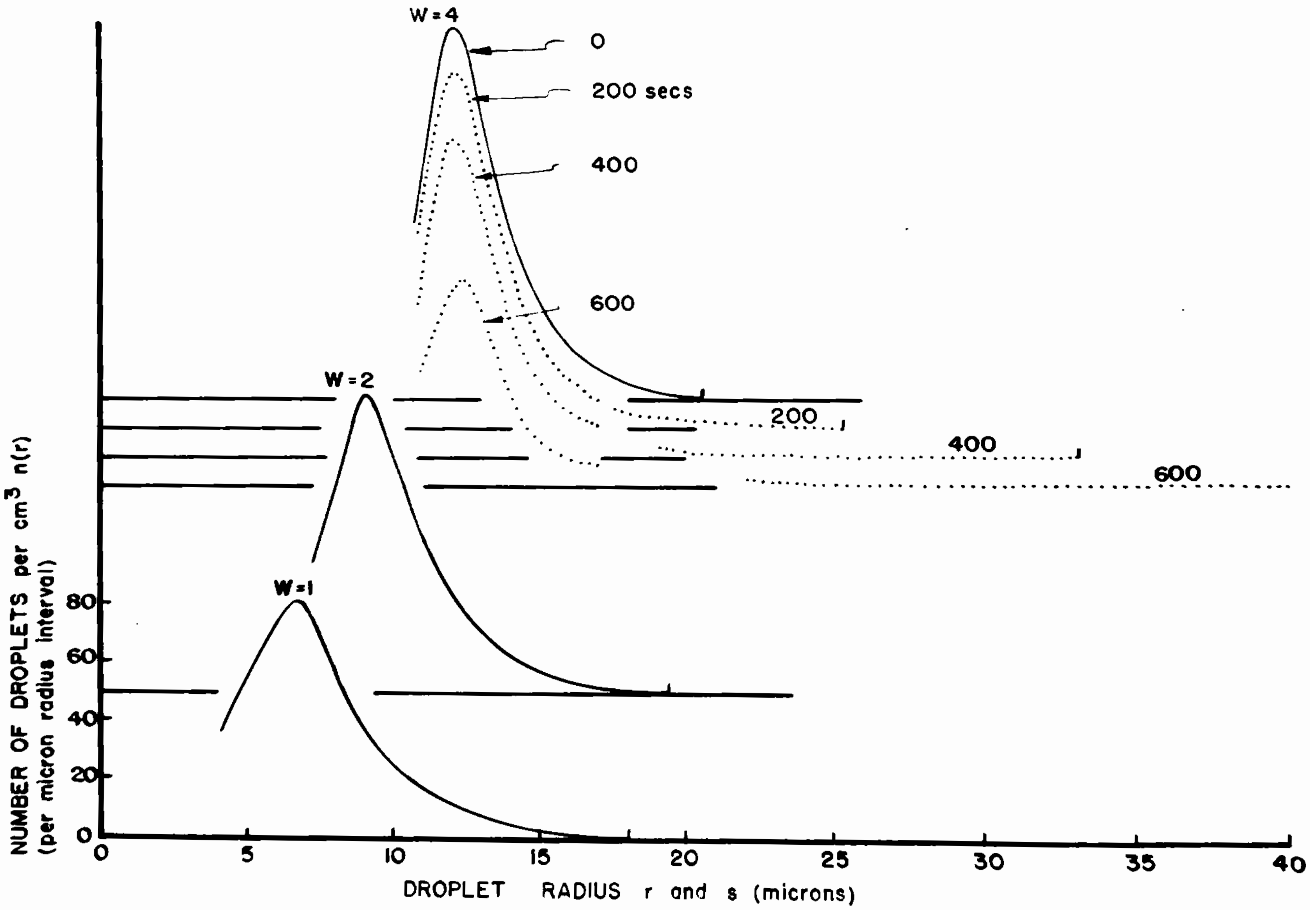

Figure 8.2 (Same as 5.4) The condensation-gravity mechanism. Solid curves: Modification of droplet number distribution by rapid condensation to 4 g m^{-3}.
Dotted curves: Further modification of droplet number distribution by gravity, at constant height. The last curve extends to 50 microns.

like a heavy cumulus (dotted curves), the largest droplets having reached 50 microns.

The mechanism just outlined would have the embryo raindrops populating the wake left by rising bubbles. The wake would give the "first echo" observed on weather radars, which Battan (1953) found was always a vertical streak a few thousand feet deep.

Such a mechanism is not inconsistent with the alternative model of an updraft with entrainment. The shear between the updraft and the environment is too great for a laminar flow to be maintained; turbulent interchange between the updraft and the surrounding cloud takes place. The parcel ascends in the core of the updraft, but at some change moment, it is replaced by air from the surrounding cloud. The parcel is ejected from the core, and, as before, gravity rapidly brings about coalescence. (Without entrainment, conditions would not be so suitable; even at a moderately low velocity like 3 m sec^{-1}, condensation acts too fast for gravity to control the drop size distribution, according to figures 5.5 and 5.6.)

8.2 Experimental verification

Experimental confirmation of these findings requires a means of detecting and tracking portions of cloud which contain populations of large cloud drops (of the order 40 microns radius). Radar is an excellent tool for this purpose since the response depends on the sixth power of radius. The first radar echoes in a precipitation-forming cumulus should be found close to the most rapidly ascending part of the cloud, at a level where the liquid water content has reached a sufficiently high value for a rapid maturing of the drop-size distribution. The echo appears at that level first, because lower down, although the cloud arrived there earlier, the water content is low and the drops grow slowly and have not yet reached detectability; higher up, the cloud has not yet arrived, or has arrived too recently.

A crucial test, then, would be to determine, from the atmospheric sounding for the day, the water content in the cloud at the first radar echo. This value of water content should be roughly independent of the properties of the air mass or of geographical factors. The work of section 3 above leads one to expect that this "first echo water content" would certainly be greater than 1 g m^{-3}, and it would not be very different from 4 g m^{-3} if figure 8.2 correctly describes the process.

Battan (1953) has already pointed out a significant coincidence between two sets of experimental results. The average height of the top of the first echo above the clpud base in Ohio thunderstorms was 10,500 ft. and in New Mexico 9,500 ft., despite wide differences in cloud temperature and altitude. Taking the mean sounding for the atmosphere in Ohio at the time of the radar observations (Byers and Braham 1949), we find that a parcel which started at the condensation level and ascended a vertical distance of 10,500 on the saturated adiabat, would contain 6 g m^{-3} of liquid water. The corresponding atmosphering sounding for New Mexico is not available at the time of writing. We would expect to arrive at roughly the same figure whenever and wherever this method is applied. It does not necessarily follow, however, that this is the actual liquid water content at that level. If bubbles were to ascend without interruption right from the cloud base, then the air contained in them would follow the saturated adiabat. In Scorer and Ludlam's model, however, those bubbles which reach the higher levels are formed part-way up the cloud from the diluted wakes of bubbles which have expired, so that at the higher levels the bubbles must have a smaller water content than a truly adiabatic ascent would give. Alternatively, on the "updraft" view, entrainment of environmental air reduces the water content to roughly 70% of the truly adiabatic value. On either view the water content at the first echo in Battan's analysis (averaged over all occurrences) must have been in the neighbourhood of 4 g m^{-3} instead of 6 g m^{-3}; the experimental figure then shows good agreement with the proposed mechanism within the uncertainty of both.

If further experimental work confirms the condensation-gravity mechanism, it should be possible to forecast, by examining an upper-air sounding, not only whether cumulus will form, but whether rain will fall. The method consists simply of examining the T-ϕ diagram to see whether a parcel, starting at the cloud base and ascending an entrained saturated adiabat, would rise to a sufficient height before losing buoyancy for the liquid water content to exceed a critical value W_1. The experimental results will have determined W_1, which appears at present to have a value of about 4 g m^{-3}.

9. SUMMARY AND CONCLUSIONS

From the observed properties of precipitating and non-precipitating cumulus clouds, the following evidence about the precipitation-forming process emerges:-

1. Rain from warm clouds shows that glaciation is not the only precipitation mechanism.

2. The impression gained, that the onset of precipitation is more closely related to, say, height above cloud base or to water content than to temperature, suggests that glaciation may not even be an important mechanism in most cases.

3. Liquid water content increases as the cloud matures. There must be continued condensation from the vapour.

4. Total droplet population decreases as the cloud matures. Coalescence must be taking place.

5. The droplet-size distribution changes radically, from one lying entirely below about 18 microns radius, to one extending up to 100 microns or more. An appreciable fraction of the droplets must be growing quite rapidly.

The untested assumption was made that Langmuir's collision theory can be applied even when the two colliding particles are similar in size, and that collision always leads to coalescence. A long series of approximate calculations then showed:-

6. Gravity, which is always present, produces coalescence,

but several times too slowly to account for observed behaviour.

7. Naturally-occurring electric charges on the droplets are too small to affect the amount of coalescence appreciably.

8. Giant salt nuclei might account for precipitation but cannot produce the observed change in distribution. Some other drop-growing mechanism is at work.

9. Turbulent motion of the cloud-filled air might reasonably account for the observations if its r.m.s. acceleration were about 3 times gravity.

10. Measurements of turbulence in clouds suitable for assessing the likelihood of 9. are lacking, but calculations based on the available data indicate that the acceleration is at least one order smaller than the required amount.

11. Continued condensation assists the coalescing action of gravity by enlarging the droplets and so making it easier for growing drops to catch them.

(a) In the core of a moderate or vigorous steady updraft, however, condensation would outweigh gravity, producing a droplet size distribution at variance with the observations.

(b) It is possible to account satisfactorily for the changes in distribution and the observed speed of growth, by supposing that some part of the cloud is first subjected to condensation until it reaches a critical water content, and is then allowed to mature under gravity without further ascent (See figure 8.2).

Conditions outlined in 11(b) above would be found in the wake of a "bubble" in Scorer and Ludlam's (1953) model for the structure of cumulus. The acceptance of 11(b), however, does not exclude the older model of updraft if the forces of entrainment are considered to act suitably.

12. The critical water content mentioned in 11(b) should be independent of temperature, latitude etc. to first order.

13. The calculations indicated that the critical water content would not be very different from 4 g m^{-3}.

14. The level at which the critical water content is reached is also the level at which first radar echoes are seen. Battan's (1952) analysis of Ohio thunderstorms then show that the critical water content is about 4 g m^{-3}.

It may be that the giant nuclei discussed by Ludlam (1951) and by Woodcock (1952) grow to raindrop size ahead of the larger population of growing cloud drops, but conditions favourable to the one favour the other process, so that rain from convective clouds usually originates from both causes. The presence of giant nuclei might, however, depress the critical water content to some extent.

If the condensation-gravity mechanism can account for precipitation from warm clouds, it may well be the main precipitation mechanism in most, and an important mechanism in all, convective clouds.

REFERENCES

Arenberg, D., 1939: Turbulence as the major factor in the growth of cloud drops. Bull. Amer. Meteor Soc., 20, 444-448.

aufm Kampe, H.J. and H.K. Weickmann, 1954: Reply to discussion. J. Met. 11, 429-430.

Batchelor, G.K., 1951: Pressure fluctuations in isotropic turbulence. Proc. Camb. Phil. Soc. 47 (2), 359-374.

Batchelor, G.K., 1954: The theory of homogeneous turbulence. Cambridge, The University Press, 197 pp.

Batchelor, G.K., 1954: Heat convection and buoyancy effects in fluids. Q.J. Roy. Met. Soc., 80, 339-358.

Battan, L.J., 1953: Observations on the formation and spread of precipitation in convective clouds. J. Met. 10, 311-324.

Bergeron, T., 1953: On the physics of cloud and precipitation. Mem. Assoc. Met. de l'Union Deodesigne, Geophysique International. Lisbon 1953.

Best, A.C., 1952: Effect of turbulence and condensation on drop-size distribution in cloud. Q. J. Roy. Met. Soc. 78, 28.

Braham, R. R. Jr., 1952: The water and energy budgets of the thunderstorm and their relation to thunderstorm development. J. Meteor. 9, 227-242.

Byers, H. and Braham, R. R. Jr., 1949: The thunderstorm. Washington, D.C., U.S. Department of Commerce. 287 pp.

Cochet, R., 1952: Evolution d'une gouttelette d'eau chargee dans un nuage a temperature positive. Ann. de Geophys.

Cunningham, E., 1910: On the velocity of steady fall of spherical particles through fluid medium. Proc. Roy. Soc. (A), 83, 357-365.

Diem, M., 1942: Messungen der Groesse von Wolkenelementen, I. Annalen der Hydrographie und Maritimen Meteorologie. May 1942.

Diem, M., 1948: Messungen der Groesse von Wolkenelementen, II. Meteorologische Rundschau, I, 262.

East, T. W. R., 1953: Turbulence in clouds as a factor in precipitation. M. Sc. Thesis, McGill University.

East, T. W. R. and J. S. Marshall, 1954: Turbulence in clouds as a factor in precipitation. Q. J. Roy. Met. Soc. 80, 26-47.

Fritz, S., 1954: Small drops, liquid water content and transmission in clouds. J. Met. 11, 428-429.

Gabilly, A., 1949: On the role that turbulence can play in the coalescence of cloud droplets. Annales de Geophysique, 5, 232-234.

Gunn, K. L. S. and W. Hitschfeld, 1951: A laboratory investigation of the coalescence between large and small water-drops. J. Meteor., 8, 7-16,

Howell, W. E., 1949: The growth of cloud drops in uniformly cooled air. J. Meteor., 6, 134-149.

Hunt, T. L., 1949: Formation of rain (letter). Meteor. Mag., 78, 26.

Kottler, F., 1950: The distribution of particle dizes. J. Franklin Inst., 250, 339-356, 419-441.

Kottler, F., 1951: The goodness of fit and the distribution of particle sizes. J. Franklin Inst., 251, 449-514, 617-641.

Kottler, F., 1952: The logarithmico-normal distribution of particle dizes: homogeneity and heterogeneity. J. Physical Chem., 56, 442-448.

Langmuir, J., 1948: The production of rain by a chain reaction in Cumulus clouds at temperatures above freezing. J. Meteor., 5, 175-192.

Ludlam, F. H., 1951: The production of showers by the coalescence of cloud droplets. Q. J. Roy. Met. Soc. 77, 402.

McDonald, J. E., 1953: Erroneous cloud-physics applications of Raoult's law. J. Meteor., 10, 68-70.

Malkus, J. S., 1954: Some results of a trade-cumulus cloud investigation. J. Meteor. 11, 220-237.

Malkus, J. S. and R. S. Scorer, 1955: The erosion of cumulus towers. J. Met. 12, 43-57.

Mason, B.J., 1952: Production of rain and drizzle by coalescence in stratiform clouds. Q. J. Roy. Meteor. Soc. 78, 377-386.

Mordy, W.A. and L.EEber, 1954: Observations of rainfall from warm clouds. 80, 48-57.

Proudman, I., 1952: The generation of noise by isotropic turbulence. Proc. Roy. Soc., A, 214, 119-132.

Ross Gunn, 1954: Diffusion charging of atmospheric droplets by ions, and the resulting combination coefficients. J. Meteor., 11, 339-347.

Sartor, D., 1954: A laboratory investigation of collision efficiencies, coalescence and electrical charging of simulated cloud droplets. J. Met. 11, 91-103.

Schiller, L., 1932: Fallversuche mit Kugeln und Scheiben, Handbuch der Experimentalphysik, Wien-Harms, pt. 4, v. 2, pp. 339-387.

Scorer, R. S. and F. H. Ludlam, 1953: Bubble theory of penetrative convection. Q. J. Roy. Met. Soc. 79, 94-103.

Smith, E. J., 1951: Observations of rain from non-freezing clouds. Q. J. Roy. Meteor. Soc., 77, 33-43.

Steinberg, J. C., H. C. Montgomery and M. B. Gardner, 1940: Results of the World's Fair hearing tests. Bell System Tech. Jour. 19, 533.

Stratton, J. A., 1941: Electromagnetic theory. New York, McGraw Hill, 615 pp.

Virgo, S.E., 1950: Tropical rainfall from cloud which did not extend to the freezing level. Meteor. Mag. 79, 237.

Weickmann, H. K. and H. J. aufm Kampe, 1953: Physical properties of cumulus clouds. J. Meteor. 10, 204-211.

Woodcock, A. H., 1952: Atmospheric salt particles and raindrops. J. Meteor. 9, 200-212.

Zaitsev, V. A., 1950: Liquid water content and distribution of drops in Cumulus clouds. Trudy Glavnoi Geofiz. Observ., 19, 122-132.

APPENDIX 1

Method of calculation for coalescence

The technique by which the result of coalescence processes was computed will be described, using as illustration the action of gravity on idealised fair-weather (I.F. cloud). The technique was modified as required in other cases.

(a) Single drop

The droplet size distribution of the cloud was broken up into 8 classes ande ach class considered to be monodisperse, as shown in figure A1.1. (The water contents in these classes are listed in Table A1.1). The behaviour of a drop of radius s in a cloud consisting of one of these classes was calculated in the following steps:

1. Calculate the terminal velocities of droplets r (equation 3.1) and of drop s (see appendix 3(b) for a steady gravitational field $g_E = 980$ cm sec^{-1}. (For three-dimensional turbulence use gravitational field $2g_E$).

2. Obtain the relative velocity between the drop s and a droplet r by subtraction, $U_1 = v_s - v_r$.

3. Calculate $K_1 = U_1 \tau_r / s$.

4. Look up E from figure 6.2.

5. Calculate the equivalent volume sweeping rate of the drop by sliderule from the equation

$$Q(s,r) = \frac{U_1 (s+r)^2}{\pi^{-1}} E \qquad \text{(A1.1)}$$

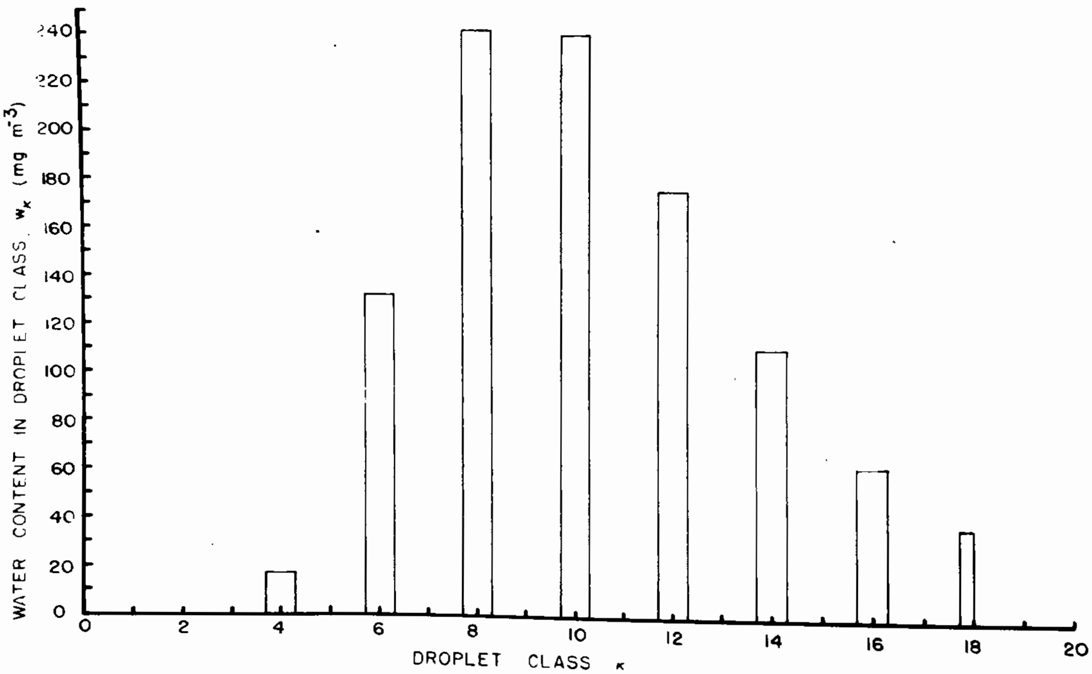

Figure A1.1 Form of I.F. distribution used in drop growth calculations. The continuous water content distribution in figure 2.3 is replaced by 8 monodisperse classes; a pillar has area proportional to the water content in that class. (See table A1.1) it is plotted in figure 3.1. (To get mean sweeping rates for turbulence, use E' or E").

6. Multiply by the water content w_K of the class K, to obtain the amount of water acquired per second by the drop from that class

$$\left(\frac{dm_s}{dt}\right)_K = w_K \, Q'(s, r_K) \tag{A1.2}$$

7. The total rate of collecting water is obtained by addition.

$$\left(\frac{dm_s}{dt}\right) = \sum_K w_K \, Q'(s, r_K) \tag{A1.3}$$

This process was carried out for about 14 values of s from 15 to 100 microns. The values were converted to mass versus time by numerical integration. It takes time $\Delta t = \frac{\Delta m_s}{dm_s/dt}$ for the drop to increase in mass by Δm_s if the interval Δm_s includes the value of m_s for which dm_s/dt has been computed. By summing the Δt's and converting from drop m_s to radius s, the curve in figure 3.3 was obtained.

(b) Drop-size distributions

To follow the development of the drop-size distribution the original idealised fair-weather distribution was divided into two parts; the larger particles are called drops, whose radii are s, and the small particles are droplets, radii r. Figure A1.2 shows the 5 classes of drops κ and the 5 classes of droplets K into which the distribution is concentrated. The boundary between drops and droplets is taken at 13 microns

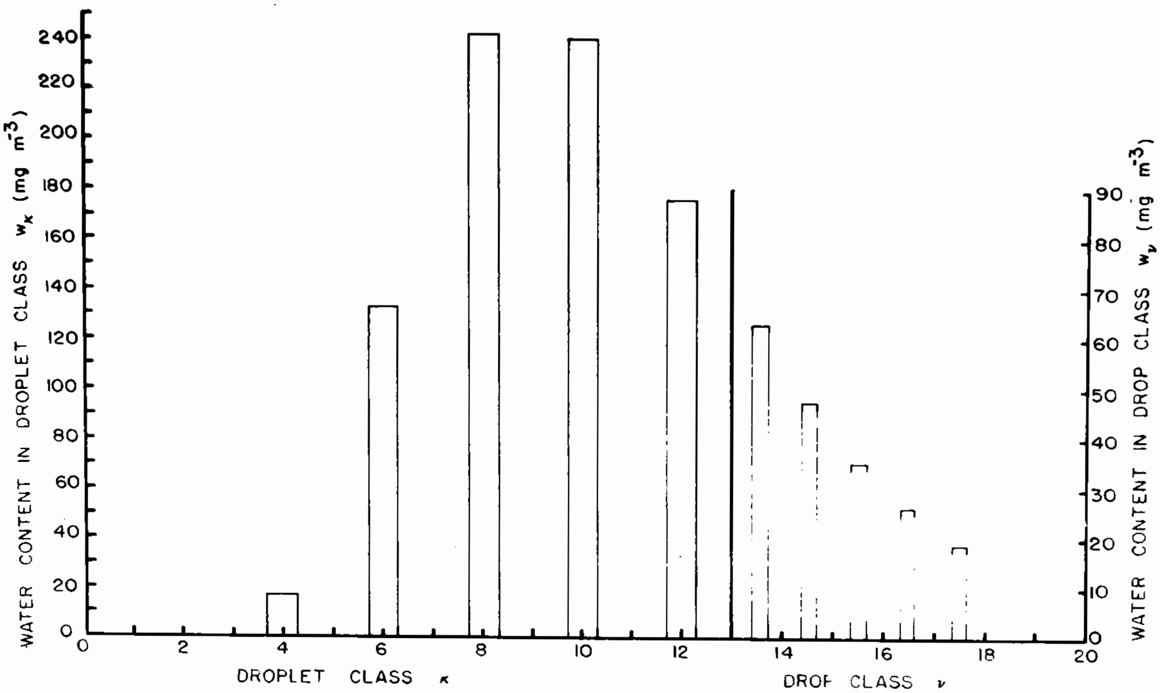

Figure A1.2 Form of I.F. distribution used in calculating modifications to droplet size distributions, The continuous water content distribution in figure 2.3 is replaced by 10 monodisperse classes; a pillar has area proportional to the water content in that class. The lower five classes contain the droplets and the upper five the drops. (See table A1.2) radius. (Table A1.2 lists the water contents in these classes. It is assumed that only collisions between a drop ($s > 13$) and a droplet ($r < 13$) occur, and that when a collision does take place the drop increases in size and the droplet loses its identity. Collisions between drops, or between droplets are assumed never to occur. This artificial restriction reduces the calculated amount of coalescence, but not, it is believed, enough to prevent the making of valid deductions from the results.

There are 25 combinations of the 5 drop and 5 droplet classes and for most of them collisions are possible between drops in class ν and droplets in class κ. As far as the drops in a certain class ν are concerned, collisions with droplets result in an increase in radius and in mass without change in number; the pillars marked ν on figure A1. 2 become taller and the corresponding radii s_ν increase. The droplets, however, can only suffer annihilation so the pillars marked κ decrease in height but the radii r_κ are unchanged.

At each stage of a calculation of modification of drop size distribution, a table is prepared with 25 squares. Along the top are the radii s_ν and the concentration n_ν of drops in each of the 5 drop classes at the beginning of a time interval Δt. Down the left-hand side are the water contents w_κ of the 5 droplet classes and other data. Each of the 25 squares contains entries relating to the transfer of water by collisions from one particular droplet class to one particular drop class.

The relevant equations in each square are

$$\frac{dm_\nu}{dt} = w_\kappa \, Q'(s_\nu, r_\kappa) \qquad \text{(A1.4)}$$

giving the gain in mass of a single drop in class ν due to collisions with class κ, and

$$\left(\frac{dm_\nu}{dt}\right)_\kappa = -\left(\frac{dw_\kappa}{dt}\right)_\nu = n_\nu w_\kappa \, Q'(s_\nu, r_\kappa) \qquad \text{(A1.5)}$$

giving the transfer of water from class κ to class ν as a whole.

The steps are:

1. Read off the quantities Q(s,r) from an expanded version of figure 3.1, entering them in the upper left corner of each square of the table.

2. Multiply along each row by w_κ, entering results at right of each square.

3. Add down each column, to obtain the growth rate for a single drop in class ν,

$$\frac{dm_\nu}{dt} = \sum_\kappa \left(\frac{dm_\nu}{dt}\right)_\kappa \qquad \text{(A1.6)}$$

4. Multiply down each column by n_ν, entering results at lower left of each square.

5. Add along each row, to obtain rate of loss of water from a droplet class κ.

$$-\frac{dw_K}{dt} = \sum_{\nu}\left(-\frac{dw_K}{dt}\right)_{\nu} \tag{A1.7}$$

A suitable time interval Δt is chosen, and the following equations applied at the bottom of the table:

$$\Delta m_{\nu} \doteq (dm_{\nu}/dt)\,\Delta t$$

$$m_{\nu}' = m_{\nu} + \Delta m_{\nu}$$

$$s_{\nu}' = (4\pi/3)^{-1/3}\, m_{\nu}'^{\,1/3}$$

where the primes signify the new values at the end of the interval Δt. These values are transferred to the top of the next table.

At the right-hand side of the table,

$$\Delta w_K = (dw_K/dt)\Delta t$$

$$w_K' = w_K + \Delta w_K$$

These values are transferred to the left-hand side of the next table. A new table is prepared for each time interval Δt. Arithmetical checks are made by totalling in various ways.

TABLE A 1.1

Idealised fair-weather (I.F.) water content distribution, as used in calculations of growth of a large cloud drop by coalescence. (See figure A1.1)

Putative class boundaries (microns)	Class radius r_k (microns)	Class water content w_k ($mg\ m^{-3}$)
3		
	4	17.3
5		
	6	133
7		
	8	240
9		
	10	242
11		
	12	176
13		
	14	110
15		
	16	61
17		
	18	19
18		

TABLE A 1.2

Idealised fair-weather (I.F.) water content distribution, as used in calculations of modification of distribution by coalescence. (See figure A1.2)

Putative class boundaries (microns)	Class radius $\cancel{r_\kappa}$ (microns)	Class water content (mg m^{-3})
Droplets	r_κ	w_κ
3		
	4	17.3
5		
	6	133
7		
	8	240
9		
	10	242
11		
	12	176
13		
Drops	r_ν	w_ν
13		
	13.5	63.2
14		
	14.5	47.6
15		
	15.5	35.5
16		
	16.5	26.3
17		
	17.5	19.0
18		

APPENDIX 2

Calculations on the condensation process

The rate at which a single droplet increases its mass when water vapour is being condensed is given by equation (5.6) as follows

$$\frac{dm_r}{dt} = \frac{r}{\sum_i r} \frac{dW}{dt} \tag{A2.1}$$

where m_r is the mass of the droplet

r is its radius

$\sum_i r$ is the sum of the radii of all the droplets per m^3

W is the liquid water content per m^3

For purposes of computation, we consider the distribution of figure A1.2 which consists of ten monodisperse classes of droplets. Multiplying equation (A2.1) by n_k, the number of droplets per m^3 in class k, gives

$$\frac{dw_k}{dt} = \frac{n_k r_k}{\sum_k n_k r_k} \frac{dW}{dt} \tag{A2.2}$$

or, in finite difference form

$$\Delta w_k = \frac{n_k r_k}{\sum_k n_k r_k} \Delta W \tag{A2.3}$$

where Δw_k is the increase in water content of class k in a time Δt, ΔW is the increase in water content of the cloud in the same time.

The working quantity in the computation is w_k, the water content of the class k.

Now $$w_\kappa = \frac{4\pi}{3} n_\kappa r_\kappa^{3}$$

so $$n_\kappa r_\kappa = (4\pi/3)^{-1/3} n_\kappa^{2/3} w_\kappa^{1/3} \qquad \text{(A2.4)}$$

The ten quantities $(4\pi/3)^{-1/3} n_\kappa^{2/3}$ were computed first, so that they were available for converting w_κ into $n_\kappa r_\kappa$ by slide rule for each class at each stage of the computation.

Starting from a table of w_κ versus κ, totalling W, each stage comprised the following steps:-

1. Convert each w_κ into $n_\kappa r_\kappa$
2. Add the column to obtain $n_\kappa r_\kappa$
3. Select a suitable value of ΔW.
4. Use equation (A2.3) to find the values of Δw_κ for each class. Total the column to check that $\sum \Delta w_\kappa$ gives ΔW.
5. In each class, add Δw_κ to the old value of w_κ to obtain a new class water content w'_κ, say. Total the column to check that the new total water content $W' = W + \Delta W$.

Figure A2.1 shows w_κ plotted against κ after each new increment ΔW. The value of total water content W is marked fo~~r~~ each stage.

The choice of increments ΔW is a compromise. Larger values of ΔW speed the work. On the other hand, the factors $n_\kappa r_\kappa / \sum n_\kappa r_\kappa$ are used for the whole of an interval ΔW whereas they are correct only at the beginning of it, and the longer the interval the greater the resulting error. From 1

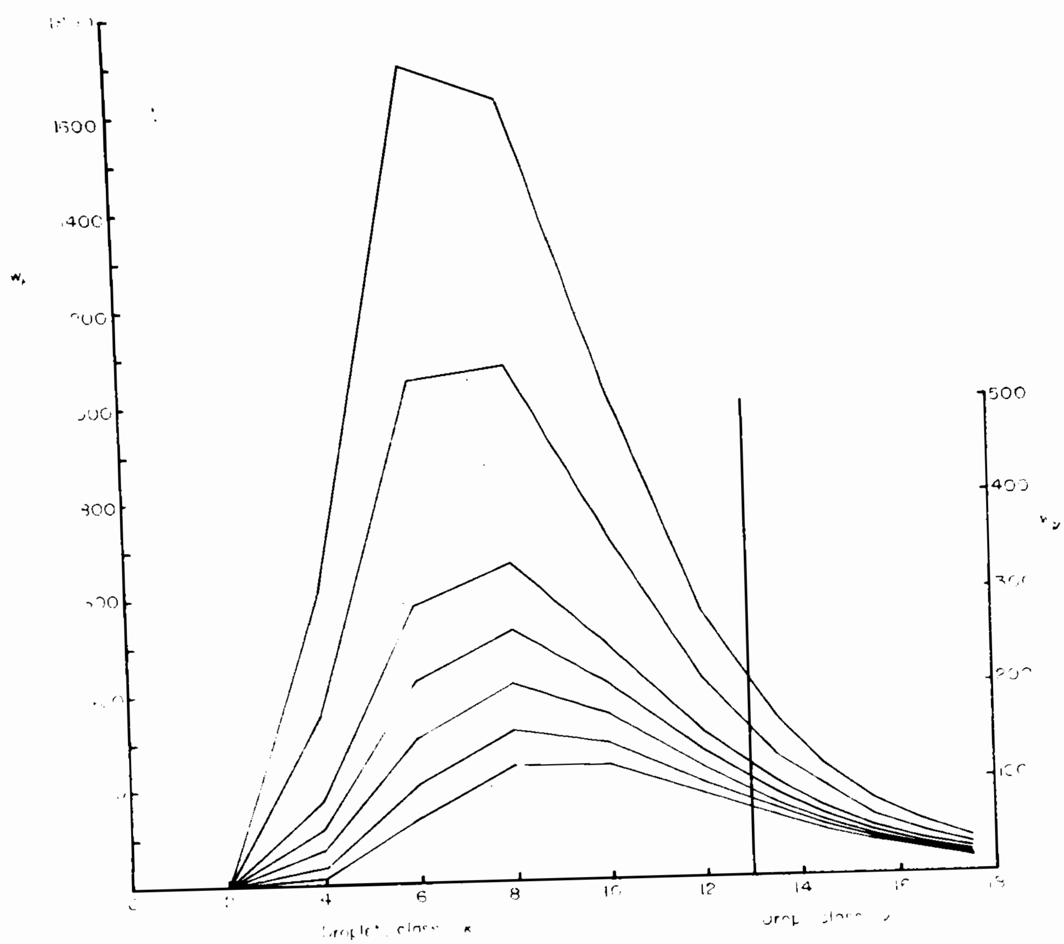

Figure A2.1 Effect of condensation on droplet classes. The lowest polygon shows the heights of the pillars in figure A1.2 ($W = 1$ g m^{-3}). The other polygons show the heights of the pillars after each step in the calculations; the water contents are $W = 1.25$, 1.6, 2, 2.5, 4 and 6 g m^{-3}. Some of them were converted to curves of water content per micron radius interval and are shown in figures 5.2 and 5.4 (8.2).

to 2.5 g m^{-3} W was increased by about 25% each time .

The effect of the size of increment can be judged from the fact that for the smallest droplets $n_\kappa r_\kappa / \Sigma n_\kappa r_\kappa$ actually increased by 16½% from W = 1 g m^{-3} to 1.25 g m^{-3}, while for the largest droplets it decreased by 8½%. This means that the computed increase in w_κ for the smaller droplets is not large enough, and for the larger droplets is too large. In fact, it shows that a more exact calculation would make the trends shown in figure A2.1 more pronounced still.

As W increased, this error diminished so that after 2.5 g m^{-3}, ΔW was made about 60% of W each time.

Figure A2.1 shows w_κ versus κ , the water content of a class versus its original radius, but for comparison with experimentally determined distributions we require w(r) versus r, that is water content per micron radius interval versus the current radius. To obtain such a distribution corresponding to one of the stages shown in figure 5.2, the actual values of r must be computed, which are best obtained from the $n_\kappa r_\kappa$'s during step 1 above. Then $w(r) = w_\kappa / \delta r_\kappa$ where δr_κ is the width of the class in microns, obtained by differencing the radii r_κ . The results at selected values of W are shown in figure 5.2. In the nature of differences, the δr_κ's showed up the limited accuracy of the computations more than the other quantities; as a result the calculated values of w(r) are actually scattered about the smooth curves shown in figure 5.2 but lie within about 5% of them.

APPENDIX 3

Approximations in the turbulence theory

(a) Frequency spectrum of turbulence

It was shown in the M. Sc. Thesis that

$$U(t) \doteq (\tau_s - \tau_r)\, A(t) \qquad \text{(A3.1)}$$

provided the frequency spectrum of the turbulent velocity satisfied the condition that above a frequency $\omega_H/2\pi$ the energy should fall off rapidly, and that at this frequency

$$\omega_H \tau_s \ll 1 \qquad \text{(A3.2)}$$

The Reynolds number R in cumulus clouds is high enough that the inertial sub-range can be assumed to exist (the terminology and notation are those of Batchelor (1953)). Then the wavenumber spectrum falls off as $K^{-5/3}$ up to a wavenumber $1/\eta$, above which it falls off as K^{-7} or some steeper law. Here $\eta = \nu^{3/4}\varepsilon^{-1/4}$. The frequency spectrum is closely related and also falls off rapidly above an angular frequency v/η , where $v = \nu^{1/4}\varepsilon^{1/4}$ Identifying this angular frequency as ω_H,

$$\omega_H = \frac{\nu^{1/4}\varepsilon^{1/4}}{\nu^{3/4}\varepsilon^{-1/4}} = \nu^{-1/2}\varepsilon^{1/2} \qquad \text{(A3.3)}$$

putting $\nu = 0.180$ cm^{2}sec^{-1} and $\varepsilon = 10^4$cm^{2}sec^{-3} (the "extreme case" of section 7.3.3) we find $\omega_H = 236$ sec^{-1}. Then $\omega_H \tau_s = 1$ for s = 45 microns. Smaller values of ε lead to slightly higher values of s.

It appears, then, that equation (A3.1) is valid for present purposes until s approaches 45 microns; after that

U is less than (A3.1) would show. Modifications of droplet size distributions (figures 6.6, 6.7, 6.11 and 6.12) are not seriously affected but curves of drop growth (figures 6.5, 6.10 and 8.1) indicate too rapid a growth after say 30 microns.

(b) Departure from Stokes' Law

The drag force D on a sphere, radius s, mass m_s, density ρ_s, moving with velocity v_s through a fluid of density ρ and viscosity η, is

$$D = \frac{\pi\rho}{2} s^2 v_s^2 C_D \qquad (A3.4)$$

where the drag coefficient C_D is a function of R, the Reynolds number. Define a factor φ such that $C_D = 24/(\varphi R)$

Then
$$D = \frac{\pi\rho}{2} s^2 v_s^2 \cdot \frac{24}{2\varphi\rho_s v_s \eta} = \frac{6\pi\eta s v_s}{\varphi} \text{ and } v_s = \frac{\varphi D}{6\pi\eta s} \qquad (A3.5)$$

Assuming the drag force $D = m_s A(t)$ (which depends on the spectrum of turbulence) then

$$v_s = \varphi \frac{2\rho_s s^2 A(t)}{9\eta} = \varphi \tau_s A(t) \qquad (A3.6)$$

where $\tau_s = 2\rho_s s^2/9\eta$

In this expression, τ_s is constant, but φ is a function of the Reynolds number R, and therefore of v_s and of A(t); it is plotted in figure A3.1, where the horizontal coordinate is drag force, which for fixed m is proportion to A(t).

To find the effect of φ on the mean efficiency E', we shall neglect the droplet velocity and suppose that the relative velocity equals the drop velocity. Consider a fixed acceleration A_o (for the present quite arbitrary), let the steady

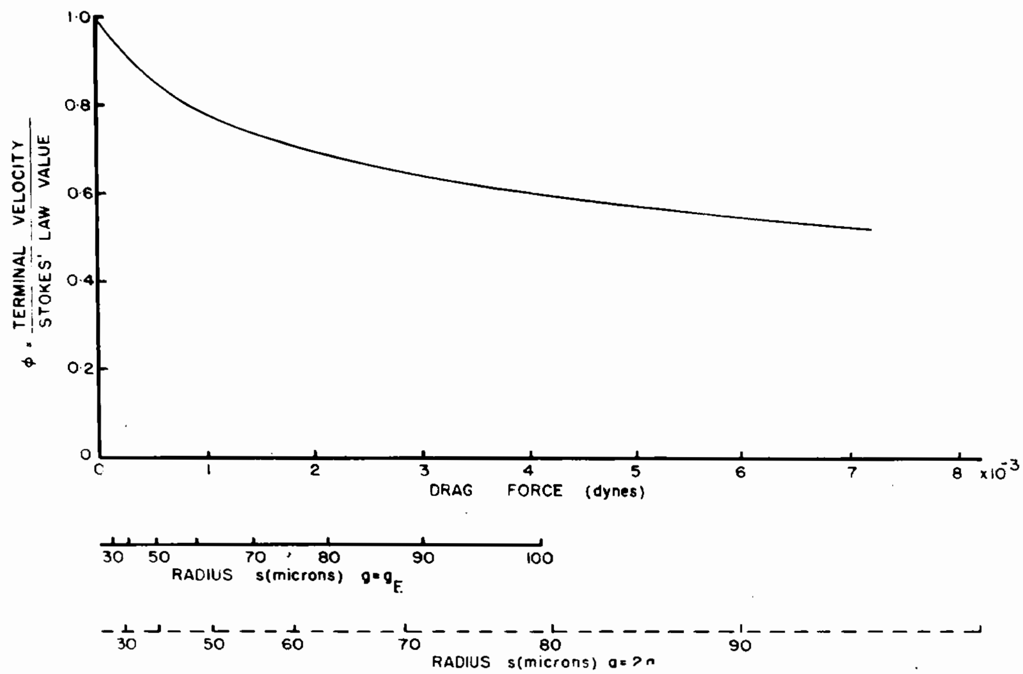

Fig. A3.1 Departure from Stokes' Law: the factor $\varphi = 24/(C_D R)$ vers drag force $D = m_s A(t)$. The curve was calculated for air 760 mb. and 0°C. Theadditional (solid) scale shows the radius of a water drop who weight is D; the dashed scale is for a doubled gravitatnal field.

velocity $U_o = \varphi_o \tau_r A_o$, and let the corresponding Langmuir parameter be $K_o = U_o \tau_r / s$. Now put reduced acceleration $a = A(t)/A_o$ A(t)A_o and reduced parameter $k = K/K_o = \varphi A / \varphi_o A_o = a.\varphi/\varphi_o$ Notice that $k = U/U_o$.

Substituting in equation (6.1) we obtain, for the mean equivalent swept volume per unit time

$$Q'(s,r) = \pi(s+r)^2 \int_0^\infty U\, E(K)\ P(U)\, dU$$
$$= \pi(s+r)^2\, U_o \int_0^\infty k\ E(k K_o)\, P(k) dk \quad (A3.7)$$

If φ were constant with time we should have $\varphi = \varphi_o$, $k = a$, and $P(k)dk = P(a)da$. The approximation consists in putting $P(k)dk = P(a)da$ regardless; the integrand then has the correct value only when $\varphi = \varphi_o$

The factor φ is plotted in figure A3.1 against drag force. The drag force is proportional to the acceleration A(t); when A(t) is below A_o, φ is greater than φ_o , and vice versa.

The exact integral can be written

$$\int_0^\infty a \frac{\varphi_o}{\varphi} . E\left(a \frac{\varphi_o}{\varphi} K_o\right) . P(a)\, da$$

The approximation consists in using instead the integral

$$\int_0^\infty a . E\,(a K_o) . P(a) da$$

The integrand has the correct value when $A(t) = A_o$, so that $\varphi = \varphi_o$. When $A(t) < A_o$, $\varphi > \varphi_o$ and the integrand in the approximate integral is too large; when $A(t) > A_o$, $\varphi < \varphi_o$ and the integrand is too small. The errors to some extent cancel if A_o is not at either extreme of the values of A(t). It was most convenient to make $A_o = gE$, for one-dimensional turbulence with gravity, since U_0 and K_0 then become U_1 and K_1, the values for gravity alone which had already been calculated for section 3. For three-dimensional turbulence, g_E lies rather low in the distribution of A, and so the value $A_0 = 2g_E$ was used; U_0 and K_0 in this case have the values U_2 and K_2.

(c) Correlation in three-dimensional turbulence

The equation of motion for an incompressible fluid makes the three components of motion interdependent, so that strictly the probability distribution of speed cannot be obtained by combining three linear velocities, without taking into account correlation between the components. Indeed, the description of turbulent motion as being made up of eddies, leads one to picture a series of circular vortices, in which the linear components are highly correlated.

However, Batchelor (1953), in section 6.1, finds that the scale life-time of the energy-containing eddies

$$\tau_e = \frac{u^2}{|d(\overline{u^2})/dt|} = \frac{1}{A}\frac{\ell}{u} \qquad \text{(A3.8)}$$

where u^2 = mean square velocity

ℓ = characteristic length of energetic eddies

A = a number (= 1.1 according to Batchelor's (1953) fig. 6.1)

Consider the eddies to have a predominant radius r_p, diameter $2r_p$, and to be packed in such a way that their characteristic wavelength is $4r_p$. The predominant wave-number $k_p = 2\pi/4r_p$, and the longitudinal integral scale is (Batchelor 1953 eq. (6.12))

$$L_p = \frac{3\pi}{4} K_p^{-1} = \frac{3}{2} r_p \tag{A3.9}$$

Assuming that L_p is a suitable substitute for ℓ , the scale time

$$\tau_e = \frac{3}{2A} \cdot \frac{r_p}{u} = \frac{3}{2A} \Omega_p^{-1} \tag{A3.10}$$

where Ω_p is the angular velocity of the eddy.

The energy of the eddy decays 1 neper in time τ_e, in which time it goes through 3/2A radians, or 95°. If L_p is too large an estimate for ℓ (as seems to be the case) the angle is proportionately reduced. Further, the major contribution to the acceleration comes from the smallest eddies in the inertial sub-range; their life-times are even less than the formula for τ_e indicates, because of viscous dissipation, so the correlation should again be decreased.

Panofsky and McCormick (1954) made extensive measurements of atmospheric turbulence 100 m above the ground. They found that the coherence (i.e. correlation coefficient between horizontal and vertical components for a particular region of the spectrum) falls below 0.10 for frequencies above 3 c/s. It seems best (and it is certainly simplest) to neglect correlation altogether in deriving P(k) for three-dimensional turbulence.